Fabrication of organic-inorganic nanocomposites by colloidal processing

By

Dan Luo, B.ENG

A Thesis

Submitted to the School of Graduate Studies in

Partial Fulfilment of the Requirements for the Degree of:

Master of Applied Science

TITLE: Fabrication of organic-inorganic nanocomposites by colloidal processing

AUTHOR: Dan Luo, B.Eng., (Southeast University, Nanjing, China)

SUPERVISOR: Prof. Igor Zhitomirsky, Distinguished Engineering Professor, Ph.D., P.Eng.

NUMBER OF PAGES: XV, 112

Abstract

Colloidal processing has been widely used for many industrial application. Electrophoretic deposition (EPD) is an important colloidal technique, which plays an important role in the fabrication of organic-inorganic composites.

In this work, advanced dispersing agents with excellent adsorption, dispersion and film forming properties have been developed. The adsorption mechanism and the deposition kinetics of EPD have been studied. It is shown that catechol and salicylic groups of dispersants can form chelation bonding with metal atoms on inorganic particle surface and provide particle charging, dispersion and deposition. The aromatic dispersants can adsorb on carbon nanotubes due to π-π interactions. The long chain ionic polymeric dispersants were investigated, which provide efficient electrosteric stabilization. The film forming properties of dispersants allow dispersants with dispersed materials to deposit and form composite films on the substrate.

Universal dispersing agents have been developed for the colloidal processing. These dispersants show possibilities to adsorb and disperse various organic and inorganic materials and pave the way for the fabrication of multi-functional materials for various applications. The composite materials, prepared using new dispersants showed promising corrosion protection of metals, flame retardant and energy storage properties.

Key words: EPD, dispersing agent, composite, adsorption, dispersion, chelate, inorganic nanoparticles

Acknowledgement

I hereby express my deepest gratitude to Professor Igor Zhitomirsky for his intellectual guidance in my way towards the nature of science. I really appreciate your supervision and I am very glad to be your student.

I would like to thank my group mates, Yisong Su, Shilei Chen, Mustafa Ata, Kaiyuan Shi, Yangshuai Liu, Tianshi Zhang, Patrick Wojtal, Jieming Li and Cameron. J. Wallar. I extend my thanks for all your help and support. I am very appreciated that I can finish my graduate study with you all.

I would like to thank Victoria Jarvis, James Britten, Chris Butcher, Steve Kornic and Frank Gibbs, thanks for your support to my research.

I would like to thank Ritch Matthews and Advanced Ceramics for their financial support for this work.

Finally, I would like to gratefully thank my family members and my dear friends for their understanding and support of my graduate studies in Canada. Thank you for always believing me and encouraging me to chasing my dreams.

Table of Contents

List of Figures

List of Tables

Declaration of Academic Achievements

This dissertation was used to fulfill the requirements of M.A.Sc degree. The major research project was undertaken from Sep 2014 to August 2016. I carried out experimental and theoretical research on developing advanced organic-inorganic materials by colloidal processing.

The results of this dissertation were published in 7 papers in peer-reviewed journals. The papers were listed below:

1 **Dan Luo**$^{\delta}$, Cameron J.Wallar$^{\delta}$, Kaiyuan Shi and Igor Zhitomirsky, (δ: These authors contributed equally to this work), Strategies for optimization of capacitive performance of MnO_2-multiwalled carbon nanotube electrodes, prepared using lauryl gallate dispersant, ***Colloids and Surfaces A: Physicochemical and Engineering Aspects,*** submitted.

2 **Dan Luo**, Tianshi Zhang and Igor Zhitomirsky, Electrophoretic deposition of tannic acid-polypyrrolidone films and composites, ***Journal of Colloid and Interface Science***, 2016, 469:177-183.

3 **Dan Luo** and Igor Zhitomirsky, Electrophoretic deposition of poly-etheretherketone composites containing huntite and alumina platelets, ***Journal of the Electrochemical Society***, 2015, 162(11): D3057-D3062.

4 Tianshi Zhang$^{\delta}$, **Dan Luo**$^{\delta}$, Patrick Wojtal, and Igor Zhitomirsky, (δ: These authors contributed equally to this work), Electrophoretic deposition of flame retardant polymer-huntite coatings, ***Materials Letters***, 2015, 159: 106-109.

5 C.J.Wallar, T.Zhang, **D.Luo**, and I.Zhitomirsky, Electrochemical and electrophoretic deposition of organic and inorganic films, ***Materials and Manufacturing Processes***, accepted.

6 Yangshuai Liu, **Dan Luo**, et al., Universal dispersing agent for electrophoretic deposition of inorganic materials with improved adsorption, triggered by chelating monomers, ***Journal of Colloid and Interface Science***, 2016, 462: 1-8.

7 Yangshuai Liu, **Dan Luo**, et al., Film deposition mechanisms and properties of optically active chelating polymer and composites, ***Colloids and Surfaces A: Physicochemical and Engineering Aspects,*** 2015, 487: 17-25.

8 Patrick Wojtal, **D.Luo**, et al., Composite polymer metal hydroxide coatings with flame retardant properties, ***Materials and Manufacturing Processes***, 2015: 1-5.

1 Introduction

The field of composite materials has attracted much attention from scientists and engineers in recent years. Composites are one of the most important engineering materials, as they offer much outstanding properties comparing to conventional materials. These materials have wide applications in areas of electrochemical, photovoltaic and energy storage devices, protective coatings and biomedical devices. Organic-inorganic composite materials are important for the purpose to fabricate high performance materials that are expected to exhibit many advanced properties. The composites show very different properties with the different proportion of each components. Thus, composite nanomaterials can achieve multifunctional properties.

Frequently people use spin-coating, dip casting to fabricate organic-inorganic composite materials. However, those techniques to fabricate nanocomposites have technological problems. Each method has certain disadvantages and technological weakness. Therefore the colloidal approach has been studied as an essential step in the tailoring of nanocomposites. Colloidal methods offer many possibilities for agglomerate free processing of nanomaterials. Colloidal techniques allow for homogeneous distribution of each component and enhance composite functional properties. This characteristic drastically increases the range of techniques to nanoparticle assembly, tape casting, slurry impregnation and EPD.

In our research, we mainly focus on the EPD method. EPD stands out as the most appropriate colloidal process to produce organic-inorganic nanocomposites by using low solid content sols and suspensions[1, 2]. Moreover, EPD method has many advantages for industrial application such as low cost, simple equipment and high deposition rate. Compared with other methods, EPD can overcome most of the drawbacks. The major challenge for EPD method is to electrodeposit electrically neutral materials. Another challenge is to avoid nanoparticles agglomeration during deposition of polymer and metal oxide particle composites. The possibility to obtain the suspension, containing well dispersed and charged particles of different materials is important for the electrodeposition process. Based on the investigation, we found new dispersing agents with strong adsorption and good dispersion abilities for advanced colloidal processing and new EPD strategies to fabricate different kind of organic-inorganic composite materials with excellent properties. Moreover, we analyzed and characterized composite nanomaterials and investigated their anti-corrosion, anti-flame and energy storage properties.

The subject of this research thus involves the development of advanced dispersing and charging agents with strong adsorption and dispersion. This work is focused on the development of new EPD methods for the fabrication of multifunctional composite materials for important application such as anti-corrosion coating, supercapacitor devices and coatings, containing flame retardants additives.

2 Literature Review

2.1 DLVO theory

The basis of DLVO theory of charged colloids has been developed by Derjaguin, Landau, Verwey and Overbeek. This theory proposed that the total pair interaction between colloidal particles includes the Coulombic double-layer repulsion and van der Waals' attraction[3].

There are some critical assumptions in the DLVO theory, such as[2]: (1) infinite flat solid surface, (2) uniform surface charge density, (3) no redistribution of surface charge, (4) no change of concentration profiles of both counter ions and surface charge determining ions, and (5) solvent exerts influences via the dielectric constant only. The DLVO considers two particles dispersed in a suspension. This theory successfully describes the interactions between two approaching particles and thus is widely accepted.

The total energy V_T of interaction of two isolated, identically charged particles can be determined as[4]:

$$\mathrm{V_T} = \mathrm{V_A} + \mathrm{V_R} \tag{2-1}$$

where V_A is attractive energy and V_R is repulsive energy. The attractive energy V_A of the van der Waals' interaction between two spherical particles can be expressed by:

$$\mathrm{V_A} = -\frac{A}{6}\left(\frac{2}{s^2-4} + \frac{2}{s^2} + \ln\frac{s^2-4}{s^2}\right) \tag{2-2}$$

in this equation, the parameter A is the Hamaker constant and s = 2 + D/r. D is the shortest distance between the two particles and r the particle radius. If D << r, Equation (2-2) can be written as:

$$\mathrm{V_A} = -\frac{Ar}{12D} \tag{2-3}$$

V_R can be derived as:

$$\mathrm{V_R} = 2\pi\varepsilon\varepsilon_0 r\, \Psi^2 \ln[1 + e^{-\kappa D}] \tag{2-4}$$

where ε is the dielectric constant of the solvent, ε_0 is the vacuum dielectric permittivity, ψ is the surface potential, 1/κ is the Debye length, which is[4]:

$$\kappa = \sqrt{\left(\frac{{e_0}^2 \sum n_i z_i^2}{\varepsilon\varepsilon_0 kT}\right)} \tag{2-5}$$

where e_0 is the electron charge, n_i is the concentration of ions with valence z_i, k is the Boltzmann constant, T is the absolute temperature. Repulsion between colloidal particles is directly related to the diffuse layer charge on the particles.

A schematic plot of V_R, V_A with distance D is shown in Figure 2-1 [5]. It shows the Van der Waals attraction energy, columbic double-layer repulsion energy, and the resultant total energy as a function of distance from the surface of a spherical particle. The DLVO theory explains the potential energy for the interaction between two particles. A peak of energy barrier is located slightly away from the surface, as the columbic double-layer repulsion energy dominates the Van der Waals attraction energy. In this case, the particles will be separated and agglomeration will be prevented. The repulsion energy is determined by the concentration and valence state of electrolyte ions which is shown in Equations (2-4) and (2-5) and the Van der Waals attraction energy is almost independent on the concentration and valence state of ions. Thus the total energy is strongly influenced by the valence state of counter-ions and concentration. The thickness of the double layer is determined by the Debye length, 1/κ. It is influenced by the electrolyte concentration. According to the DLVO theory, there is a critical electrolyte concentration (flocculation value) for coagulation, which reduces with the valence state of the electrolyte ions of a charge opposite to that of the colloidal particles[6]. It was illustrated that the energy barrier reduces with the electrolyte concentration increases. As the potential energy peak below than zero, coagulation happens as shown in Figure 2-2 [4].

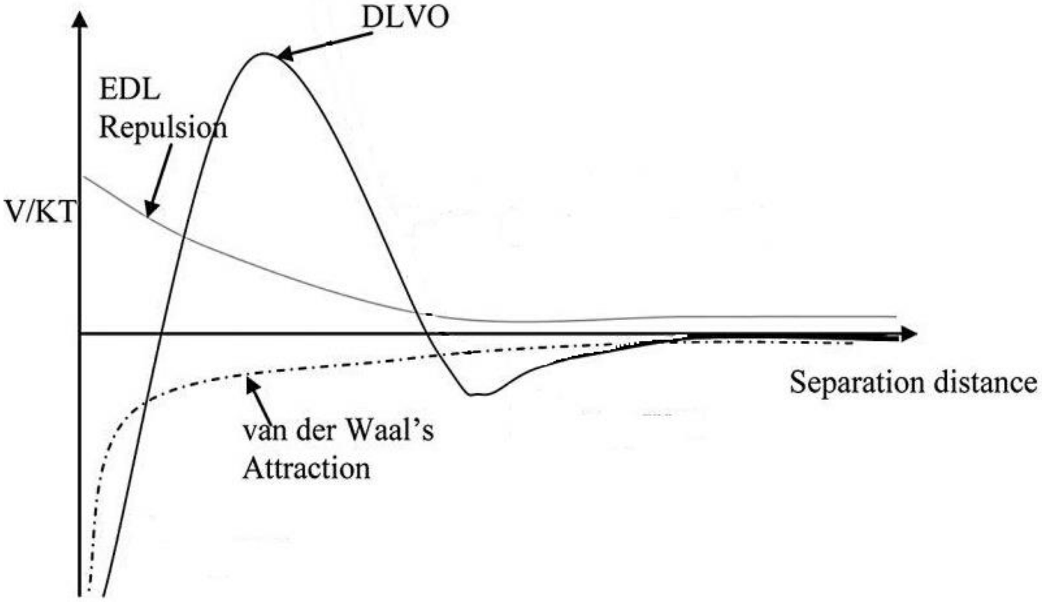

Figure 2-1 Schematic of the interaction energy as a function of separation between two particles in suspension[5]

Flocculation by ions compressing the thickness of double layer also satisfies the Hofmeister series[6]. So at the same valence, compared to small cations, a negatively charged sol is flocculated by large cations at a smaller concentration[4]. Besides, the Flocculation values has many influencing factors such as the concentration, temperature and particle size etc.

Recent studies showed that geometrical confinement can cause an important effect on the interaction between particles, for example long-range attractions, which are not considered in the DLVO theory[7]. Other forces like electro-hydrodynamic flows-induced interaction, polarization interaction and capillary interactions can also exist in the system.

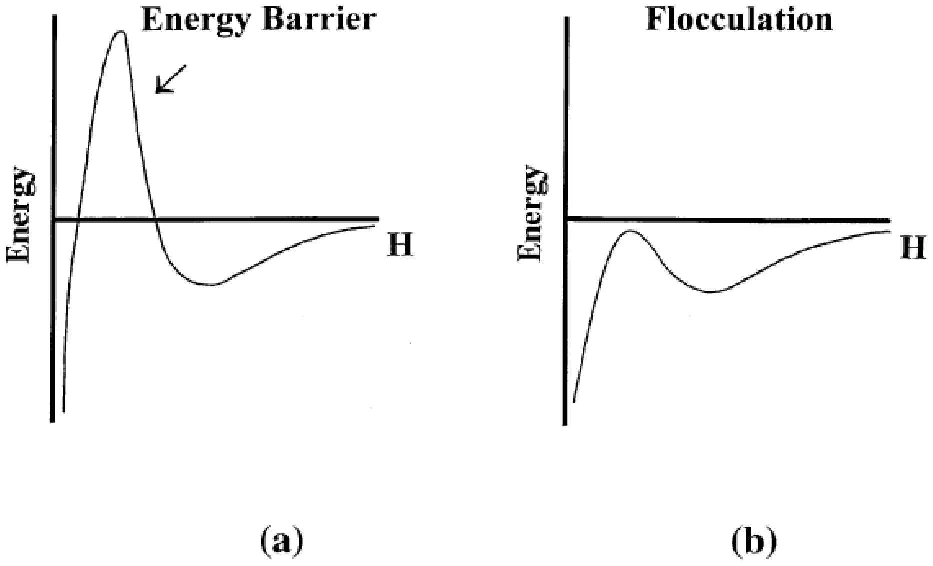

Figure 2-2 Total interaction energy between spherical particles as a function of particle separation at (a) low and (b) high electrolyte concentrations[6]

2.2 Suspension stability and particle charging

2.2.1 Double layer and zeta potential

For colloidal system, the most important thing is to well disperse particle and form a uniform suspension. So it is critical to gain well dispersed and stable suspensions.

The charged particles in a suspension are forced to move toward electrode with opposite charge under the influence of an applied electric field. This process is called electrophoresis.

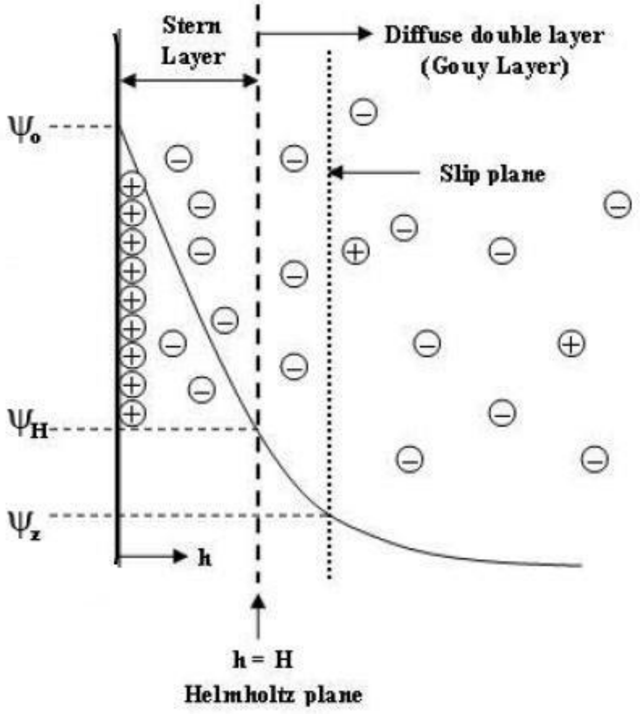

Figure 2-3 Schematic illustrating electrical double layer structure and the electric potential near the particle surface[2]

Usually, charged particles in a suspension are covered by counter ions, and the concentration of counter ions is much higher near the surface of the particles and decreases with the distance increases. Such inhomogeneous distributions of ions close to the particle surface result in the formation of so called double-layer, as shown in Figure 2-3 [2]. The double layer is composed of Stern layer and Gouy layer, and these two layers are separated by Helmholtz plane (h = H). The electric potential near the surface decreases linearly in the Stern layer. However, in Gouy layer, the counter ions diffuse freely and the potential does not decrease linearly.

The motion of these ions and the particle in opposite directions is expected when an electric field is applied. Some ions are also attached to the particle. In this case, a fraction of these ions that surround the particle will not move in the opposite direction but move along with the particles. The potential at the boundary between the electrolyte solution moving with the particle and the electrolyte solution, which does not move with the particle, is called the zeta-potential, ψ_ζ, which is explained in Figure 2-4 [8]. Zeta-potential is the principal parameter determining the electro-kinetic behavior of the particle. Basically, a particle with a negative surface charge can show a positive zeta-potential.

For aqueous suspensions of ceramic particles, especially metal oxides, the ζ potential changes with pH value if H^+ and OH^- are potential-determining ions, showing an isoelectric point (IEP), as illustrated in Figure 2-5 [4]. Zeta-potential is positive at low pH condition and negative at high pH condition.

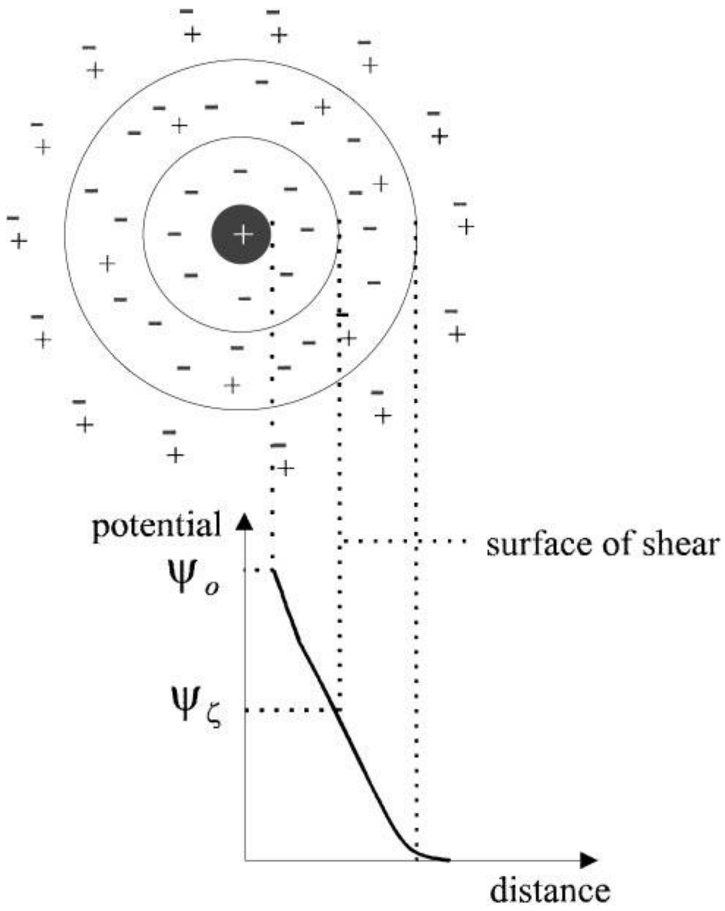

Figure 2-4 Schematic of the double layer surrounding a charged particle and evolution of the electric potential from the surface potential, ψ_0, to zero far from the particle[9]

According to the DLVO theory, ζ potential is very important for the stability of colloidal dispersions and stabilization. The ζ potential indicates the degree of repulsion between adjacent, similarly charged particles in the dispersion. A high ζ potential suspension usually has high stability. However when the potential is low, attraction overcomes repulsion and the dispersion will break and flocculate. So, colloid system with high ζ potential are electrically stabilized while colloid system with low ζ potentials are easily to coagulate.

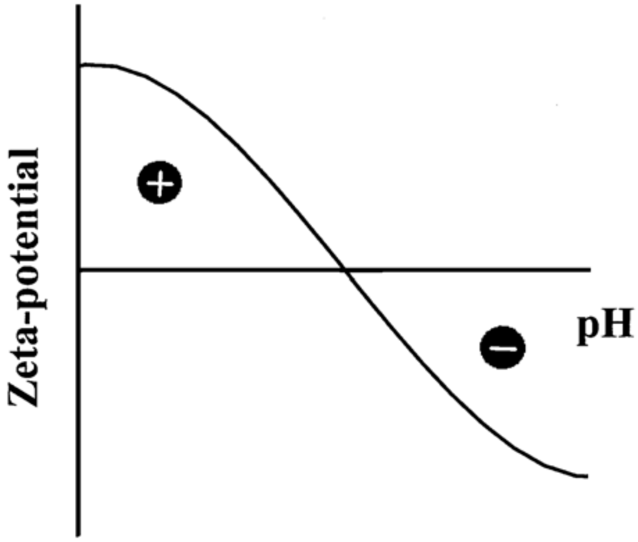

Figure 2-5 Zeta-potential of ceramic particles versus pH of suspension[4]

2.2.2 Stabilization

In order to maintain the stability of the colloidal suspension, the repulsive force must be dominant. There are three main mechanisms, electrostatic, steric and electrosteric stabilization, which are shown in Figure 2-6. The three mechanisms are very essential when hydrophilic molecules are absorbed or bounded to the particle surface.

The electrostatic stabilization is generally based on the mutual repulsion of like electrical charges which is well described before. The steric stabilization involves the adsorption of polymers onto the particle surface. If enough polymers are adsorbed, the layer of polymer is thick enough to keep particles separated by the steric repulsion between the polymer layers, the repulsion force can overcome the van der Waals attraction forces and prevent particle agglomeration. Some polymers can present both electrostatic and steric stabilization when combined with appropriate functionalities. Such polymers provide electrosteric stabilization. The steric stabilization forces are commonly short-range force which electrostatic force dominates long-range repulsion. Ionic polymeric dispersants are very sensitive to the pH and the ionic strength of solutions[10].

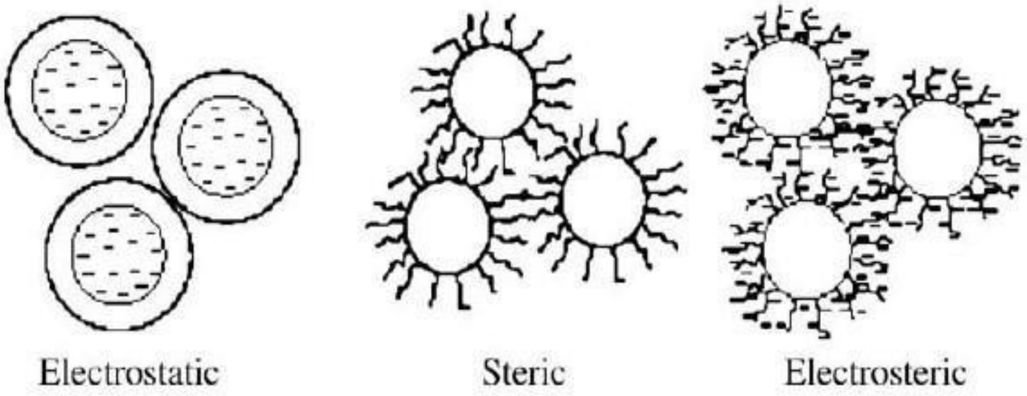

Figure 2-6 Schematic of three major stabilization mechanism[10]

Compared to the electrostatic stabilization, steric stabilization system is very difficult to flocculate if it is required. However, adding polymer will bring some undesired property to the suspension and may cause undesired side effect. Meanwhile, during the processing or sintering of those polymer adsorbed ceramic material, those polymer additives will decompose or burn out, which results in shrinkage and defects in the finished cast.

2.2.3 Influence of solvents on particles charging

In aqueous suspension, the charge at the particle—solvent interface could result from adsorption or desorption of ions, or dissociation of surface groups.

It is known that metal oxide is often fully or partly covered by OH groups. Metal oxide particles show an isoelectric point if H^+ and OH^- are potential-determining ions. Depending on the pH of the solution, they are positively charged at low pH, and negatively charge at high pH:

$$\mathrm{M-OH+H^+ \Leftrightarrow M-OH_2^+} \tag{2-6}$$

$$\mathrm{M-OH+OH^- \Leftrightarrow M-O^- + H_2O} \tag{2-7}$$

Particle charging is accomplished by electron transfer between the solvent and particle in non-aqueous media[11]. The charge on a colloidal particle could come from the solvent. Different solvents will have different charging mechanisms, for example, ethanol, water, organic acids are viewed as proton donors and are essential for particle charging. A mixture of solvents will also be helpful to accomplish particle charging[12].

2.2.4 Additives for particle charging

Particle charge could also be achieved by using various additives in order to get well-dispersed and stable suspensions. Acids[13, 14] could strongly adsorb and disperse the particles and promote the particle charging. But acids would cause corrosion of electrodes. Moreover, some acids can react with powders. It is found that a mixture of acetone, iodine and water can efficiently charge particles[12, 15]. Particle charging was carried out by the adsorption of protons ionized from solvent. The charging of ceramic particles could be accomplished by the adsorption of inorganic cations on its surface such as Mg^{2+} and Ca^{2+} [16]. Meanwhile, the charging of inorganic particles can be achieved by the adsorption of ions from the solutions of metal salts. However, metal ions, adsorbed on the colloidal particles, usually participate in electrode reactions and incorporate into the deposits as corresponding hydroxides or oxides[4].

Steric stabilization, also known as polymeric stabilization, is widely adopted in stabilization of colloidal dispersions. Steric stabilization is an efficient way to disperse particles and it is superior to electrostatic stabilization mechanism in the synthesis of nanoparticles, especially when narrow size distribution is demanded. Polymer could be used to produce steric stabilization, in which the multiple functional groups of macromolecules in each monomers provided many adsorption sites to adsorb on the particle surface. It is effective for steric stabilization in both aqueous and non-aqueous suspension.

2.3 Electrophoretic deposition (EPD)

Electrophoresis was invented by the Indian scientist G. M. Bose during the 1740s in a liquid-siphon experiment. In 1807, the Russian Reuss first observed the phenomenon that solid particles (clay) in water move under electric field[17]. However, electrodeposition indeed took off with the development of effective electrolytes for silver and gold deposition in the 1840s. These have been the basis of an extraordinarily successful decorative plating industry[18]. Electrodeposition of organic and inorganic materials can be achieved by anodic or cathodic deposition methods. Two processes are commonly used to prepare organic and inorganic coatings: the electrophoretic process (EPD) and the electrolytic process (ELD). EPD is based on the use of suspensions of ceramic particles or polyelectrolytes while ELD starts from solutions of metal salts. The range of thickness of coating fabricated by these techniques is shown in Figure 2-7[4]. EPD enables the formation of relatively thick films, whereas ELD is an important techniques for the preparation of thin films.

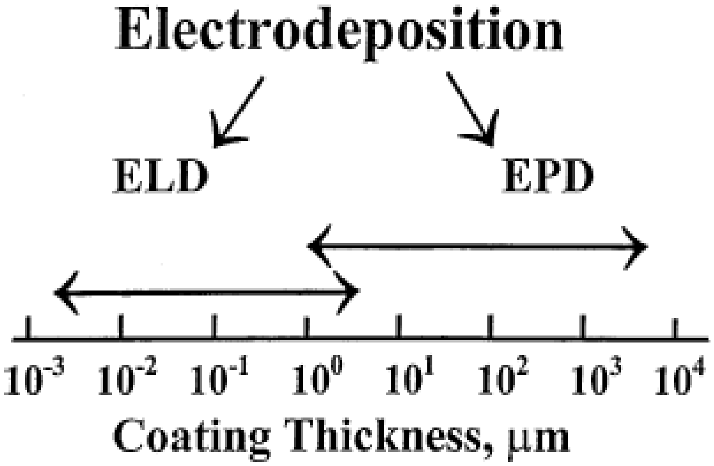

Figure 2-7 Thickness of coatings deposited using EPD and ELD[4]

EPD is an electrochemical method which has attracted substantial attention for the fabrication of thin films of ceramic, metal, composite materials for industrial applications and increasing interest as a material manufacturing and processing technique. It is a promising technology and it is an economic way to fabricate relatively thick coating comparing to electrodeposition. Generally, EPD is defined as the deposition of a substance on an electrode by the action of charge species moving under the influence of electric field and activity, especially by electrolysis[4, 19].

EPD is widely used for coating application, but there are also new and advanced applications using different templates, which can be used for the fabrication of nanocrystals, nanowires, composite materials, etc. EPD is a combination of two processes: electrophoresis and deposition. Electrophoresis is the motion of charged particles in a suspension toward an electrode under the influence of an electric field. In a second step the particles accumulate on the surface of electrode and deposit a relatively compact and homogeneous film. The EPD process is shown in Figure 2-8[17]. It is important to know that electrode reactions are not involved in the EPD[8].

Compared to other advanced techniques, EPD process is quite versatile because it could be easily modified for a specific application. The advantage of EPD is based on its high versatility to be used with different materials and combinations of materials. Meanwhile, EPD provides much advantages for surface modification over other techniques. Also, EPD can produce uniform and dense coating. Furthermore, it is easy to deposit wide range of materials on any substrates with relatively high deposition rate. For instance, any shape of substrates of complex shape demanded could be used for the EPD only if minor adjustment in terms of the electrode design and positioning is made. Especially, through control of the deposition time, concentration of material and dispersant or applied voltage, the thickness and mass could be readily modified. Furthermore, EPD techniques can achieve high purity of deposited materials at very low cost. All these properties and advantages contribute to a significant interest in the application of EPD techniques for the fabrication of films and coatings composing organic and inorganic nanomaterials.

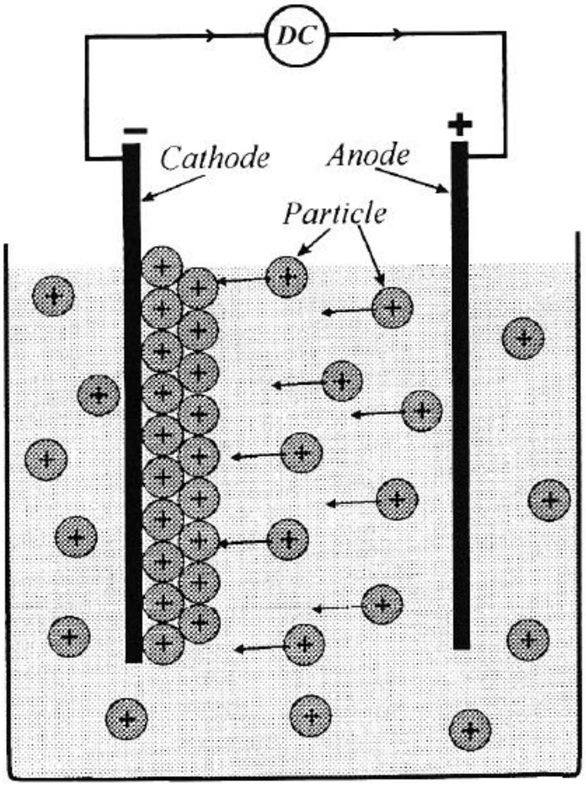

Figure 2-8 Schematic drawing of EPD cell showing the process[17]

There are two types of EPD process depending on which electrode the deposition happens, as it is shown in Figure 2-9. When the particles are positively charged, under the influence of applied electric field, the particles will move to cathode and form the deposition on the surface of cathode. This process is called the cathodic EPD (Figure 2-9 a). Similarly, the deposition of negatively charged particles on the anode is named the anodic EPD (Figure 2-9 b). However, due to the problem of anodic oxidation and dissolution of the metallic substrate when applied the anodic EPD in aqueous suspensions, measurement of anodic deposit mass becomes more difficult. Therefore, cathodic EPD is frequently used in coating fabrication area.

In several experiments, EPD of ceramic particles was performed in the presence of electrolytes and polyelectrolytes. Presently, various electrochemical methods draw much attention for broad range of study, which are based on the EPD of polyelectrolytes and inorganic particles.

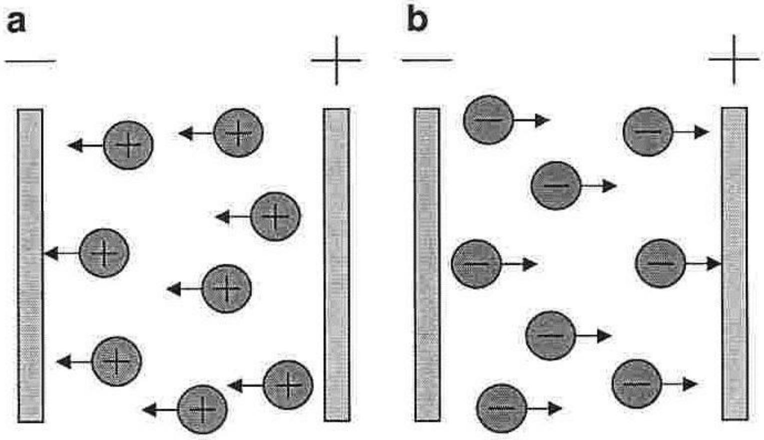

Figure 2-9 Schematic of electrophoretic deposition process. (a) Cathodic EPD; (b) Anodic EPD

2.4 Kinetic study of EPD

The deposition rate is critical for film formation and thickness control of the deposited film during EPD. Besides, deposition rate is also important for functional material design[20]. Since the EPD was established, the kinetics study of EPD has attracted much attention to investigations. In 1940, Hamaker conducted the experiment of the EPD process and observed that the mass of deposits is proportional to the concentration of the suspension, deposit time, surface area of the deposit, etc. The relationship can be written in the following equation[9, 21]:

$$\frac{dY}{dt} = \mu ESC \tag{2-8}$$

where Y is deposition yield (kg), t is deposition time (s), μ is electrophoretic mobility ($m^2 \cdot v^{-1} \cdot s^{-1}$), S is the surface area of electrode (m^2) and C is concentration ($kg \cdot m^{-3}$). This equation is known as the Hamaker equation and it is now viewed as the fundamental theory for EPD kinetics.

The velocity ν of a particle under the influence of an electric field E is defined as:

$$\nu = \mu E \tag{2-9}$$

There are two different theories to determine electrophoretic mobility μ for rigid particles and for polyelectrolytes[22, 23]. For rigid colloidal particle, μ can be given by the following equation[24]:

$$\mu = \frac{2\varepsilon\varepsilon_0\zeta}{3\eta} f(\kappa\alpha) \tag{2-10}$$

where η is the liquid viscosity. The function f(κα) increases from 1 for $\kappa\alpha << 1$ to 1.5 for $\kappa\alpha >> 1$. And for particle size which are smaller than the Debye length, the electrophoretic mobility is described by Huckel equation[4]:

$$\mu = \frac{2\varepsilon\varepsilon_0\zeta}{3\eta} \tag{2-11}$$

For particles that are larger than Debye length, μ is given by Smoluchowski equation[4]:

$$\mu = \frac{\varepsilon\varepsilon_0\zeta}{\eta} \tag{2-12}$$

On the other hand, the electrophoretic mobility of a spherical polyelectrolyte, in which fixed charges are uniformly distributed on its surface, can be given by the following equation[25]:

$$\mu = \frac{\rho_{\mathrm{fix}}}{\eta\lambda^2}\left[1 + \left(\frac{\lambda}{\kappa}\right)^2 \frac{1+\lambda/2\kappa}{1+\lambda/\kappa}\right] \qquad (2\text{-}13)$$

where charge density is ρ_{fix} and $\lambda = \left(\frac{\gamma}{\eta}\right)^{0.5}$, γ is the frictional coefficient of the polyelectrolyte.

Comparing equation (2-10) with equation (2-13), there is a concept of zeta potential, which was developed for rigid particles. As for polyelectrolytes, we cannot define zeta potential in the system so we use charge density instead of zeta potential.

2.5 Dispersing agent

The major concern for colloidal processing is to disperse particles in suspension, provide charge and then allow for EPD. However, dispersing agent can easily adsorb on particles and stabilize particles in suspension. The advantage of using dispersing agent is that dispersing agent can provide efficient electrostatic repulsion or steric repulsion between the particles. Some dispersing agents have anionic or cationic properties so that those charge species can move toward the electrode under the influence of an electric field. A critical property of a dispersing agent is its adsorption on the particle surface. An adsorbed ionic dispersant imparts a charge to the particles so that particles can be deposited under electric field. However, a non-adsorbed ionic dispersing agent acts as an electrolyte. It increases the ionic strength of the suspension, decreases the electrostatic repulsion of particles and promotes agglomeration. The increase in the ionic strength results in increased conductivity of the suspensions, enhanced gas evolution at the electrode and significant pH changes at the electrode surface. The pH change at the anode or cathode can lead to decreasing charge or charge reversal of the particles near the electrode surface. To well disperse and stabilize particles, there is a strong need in the development of advanced dispersing agents with strong adsorption to inorganic particles.

Recently, a newly developed adsorption mechanism has published in Science, which is inspired by the adhesive proteins of mussels[26]. Mussels could attach to almost all types of organic and inorganic surfaces[27]. A new research to develop efficient dispersing agents with strong adsorption to the particle surface evolved from the investigations of surfaces adsorption mechanism of mussels[26, 28, 29]. Mussels show excellent adhesion to different surfaces in saline water. The very strong and fast adsorption of mussels to different surfaces[28] prevents their damage by sea waves. Many studies[28, 29] showed that strong mussel adhesion relates to protein macromolecules, containing catecholic amino acid, L-3,4-dihydroxyphenylalanine (DOPA), a catechol family molecule. The important advantage of the catechol family is its high binding strength under wet conditions[30]. The adhesion mechanism of mussels is attributed to the complexation of metal atoms on material surfaces by OH group of the catechol ligands (Figure 2-10). The catechol has two OH group which bond on the adjacent carbon atom on the aromatic ring. In this case catechol can form chelation with different kind of inorganic materials and strongly adhere to different substrates. DOPA (Figure 2-11 a) provides bidentate interfacial interactions with different materials, containing metal atoms[28, 31] in both low pH and high pH solutions with complete protonation of amino group or deprotonation of the OH groups[32, 33], which in turn, provide charge for particles and form stabilized suspension. These studies generated significant interest in the use of DOPA for the fabrication of synthetic polymer adhesives[30, 34-36]. The fundamental study of mussel adhesion has driven the development of dispersing agents from the catechol family of molecules to make stable suspensions of colloidal particles[37]. The use of DOPA in EPD presents difficulties due to zwitterionic properties of this molecule.

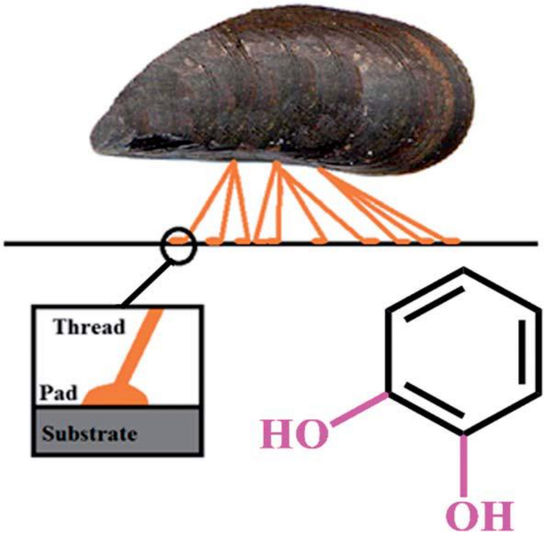

Figure 2-10 Schematic of mussel adsorption and chemical structure of catechol[37]

However, some molecule with similar structure of DOPA such as dopamine and caffeic acid(CA), which only have one functional group to provide charge, can be utilized in EPD of inorganic particles. The amino group of dopamine (Fig 2-11 b) can be protonated in solutions of inorganic acids. As a result, dopamine exhibits cationic properties in acidic solutions. Dopamine was used for dispersion and cathodic EPD of inorganic materials such as TiO_2, MnO_2, ZnO[38-40] from suspensions in ethanol or in ethanol–water mixture solvent. It was found that dopamine can be used to fabricate composite materials. Dopamine can be used as a cationic dispersing agent to co-disperse different components. The feasibility of the new approach was demonstrated by co-deposition of TiO_2 and MnO_2[40], and MWCNT[39]. It was found that EPD of ceramic particles, containing adsorbed dopamine as a charging and dispersing agent, can be combined with the EPD of cationic polyelectrolytes to make organic–inorganic nanocomposites[38].

Caffeic acid (CA) has carboxylic group on its chain so that it exhibits anionic properties (Fig 2-11 c). CA showed strong adsorption on inorganic surfaces, such as stainless steel[41], TiO_2[42, 43], SiO_2[44, 45], ZrO_2[46] and MnO_2[46] in different solvents. The strong adsorption of CA on inorganic particles can involve phenolic and carboxylic bonding sites[46]. It paves the way for the wide applications of CA for nanoparticles synthesis and dispersion. The use of CA for charging, dispersing and deposition of TiO_2, MnO_2 and ZrO_2 nanoparticles can easily form uniform and dense deposits on various conductive substrates[43, 46]. It was found that CA can be used as a co-dispersant for anodic deposition to fabricate ceramic coating and composite films. Investigations showed that composite MnO_2–zirconia films can be formed by EPD method using CA as co-dispersing agent. Film composition can be easily modified by changing the concentration of MnO_2 and zirconia in the suspensions[46].

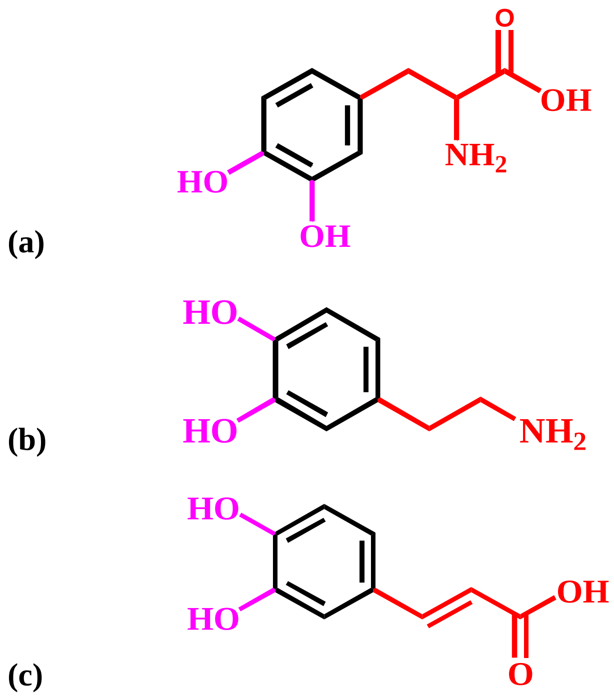

Figure 2-11 Chemical structure of (a) DOPA, (b) dopamine and (c) caffeic acid

Many other organic molecules and other functional group with chelating properties can be used. A number of investigations show that salicylic acid, gallic acid and chromotropic acid family molecule[37] exhibit strong adsorption on inorganic particles and excellent charging, dispersing properties to stabilize particles in suspension. Figure (2-12 a) shows a chemical structure of salicylic acid (SA). The positive charge of SA is related to ionization of COOH group. SA showed adsorption on TiO_2[47], MnO_2[48], ZrO_2, Al_2O_3, and Ta_2O_5[49]. EPD of MnO_2 and TiO_2 was performed using SA as a charging and dispersing agent in ethanol solvent[48, 50].

Figure (2-12 b) shows a chemical structure of gallic acid (GA), which includes three OH groups bonded to adjacent carbon atoms of the aromatic ring and a COOH group on the other side. Similar to catechol family, the OH groups provided strong adsorption of GA on various metal oxides. The anionic properties of GA are related to COOH group[37]. The investigation showed that GA chemisorbs by complexation through two OH groups[51]. The third OH and COOH groups did not influence much the stability and adsorption properties. The use of GA to disperse and charge MnO_2 in suspensions allowed for very good stability and anodic films were obtained on various conductive substrates by the EPD method[50, 52, 53]. The comparison of the EPD yield data and FTIR data for MnO_2 and TiO_2 suspensions using GA and benzoic acid confirmed the importance of phenolic OH groups for GA adsorption[54].

The structure of chromotropic acid (CHR) is shown in Fig (2-12 c). The negative charge of CHR comes from two SO_3^- group[37]. CHR can form complexes with different metal ions and shows good adsorption on different inorganic surfaces[53, 55, 56]. The use of CHR allowed the fabrication of deposits from stable suspensions with uniform and adherent properties. The deposition yield was well controlled by variation of deposition voltage, time and concentration of particles and CHR.

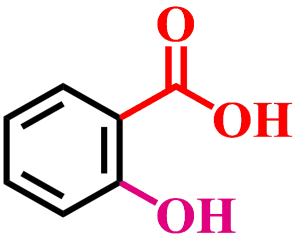

(a)

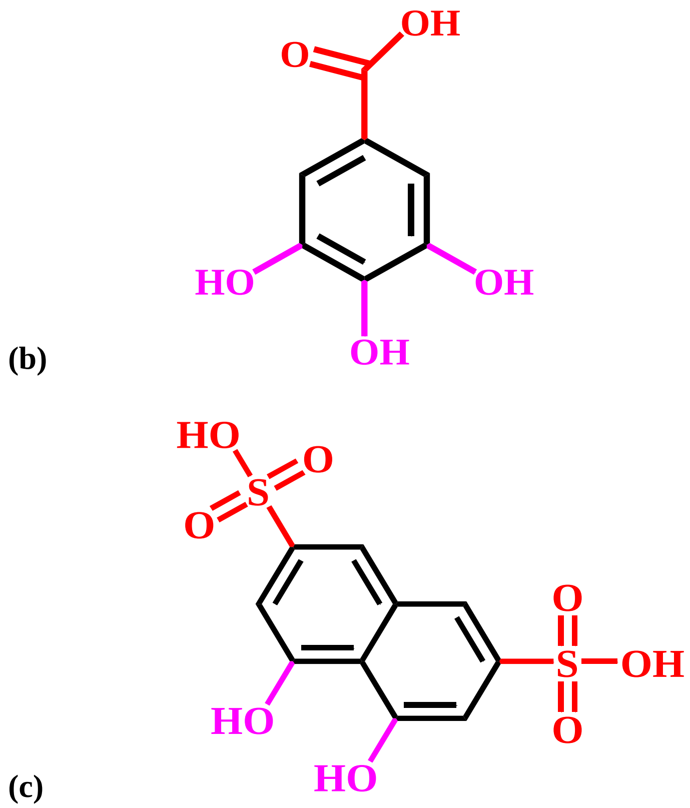

Figure 2-12 Chemical structure of (a) salicylic acid, (b) gallic acid and (c) chromotropic acid

2.6 Deposit film formation

Understanding film formation mechanisms is crucial to the development of thin film coatings. In EPD method, film formation is a two-step process, which includes the electrophoretic motion of charged inorganic particles towards the electrode and deposit formation. Many film formation mechanisms of EPD have been discussed in recent publications[57-59]. One hypothesis is that charged particles move toward the electrode, undergo reaction which neutralize them. Particle and electrode do not react and ceramic particles do not immediately lose their charge once deposited. When applied reversal electric field, the deposited layer will strip off[57]. Many investigations have approved that opinion and tried to develop a method to decrease the particle's electrostatic repulsion at the electrode and accomplish composite coating of inorganic particles with uniform and dense structure[19]. The ability to deposit monolayers or separate particles suggests that particle-electrode interactions could result in deposit formation.

Hamaker and Verwey[60] proposed another theory that the formation of a deposit by electrophoresis is similar to the sediment formation under gravity. It was supposed that applied electric field exerts sufficient force to overcome particle electrostatic repulsion. On the other hand, Verwey and Overbeek[61] pointed out that the electric field strength applied in EPD cannot overcome particle mutual repulsion but enough to bring particle near the electrode surface. The concentration of water and electrolyte in the bath are very important for EPD process. A theory proposed[62] that reduction of water (Equation 2-14) near cathode generates OH^- and cause pH increase. Even the electrode blocking by the deposited particles could also result in pH increase near the cathode[63].

$$2\mathrm{H_2O} + 2e^- \rightarrow \mathrm{H_2} + 2\mathrm{OH^-} \tag{2-14}$$

Therefore, it is important to discuss the contributions of different proposed mechanisms at different stages of EPD. Interparticle forces, electrode reactions, solvents and additives could influence the formation of thin film coating.

2.7 Deposition of polymers

A number of researches are focusing on the development of new polyelectrolytes. Comparing to traditional electrolyte, polyelectrolytes can offer both steric and electrostatic stabilization, efficiently disperse particle and form uniform suspension. Moreover, polyelectrolytes are utilized for particle charging because of the charged functional groups. They can be divided into two categories: strong polyelectrolytes and weak polyelectrolytes[64]. For strong polyelectrolytes such as poly(diallyldimethylammonium chloride) (PDDA)[4], the degree of ionization is independent of the solution pH. However, the degree of ionization of weak polyelectrolytes depends on its solution pH[4] such as poly(allylamine hydrochloride) (PAH), chitosan (CHIT), which contain amine groups[65, 66]. Strong polyelectrolyte provides both electrostatic stabilization and steric stabilization, while weak polyelectrolyte has more contribution in steric stabilization.

2.8 Organic-inorganic composite co-deposition

Composite co-deposition means the fabrication of composite coatings containing inorganic nanoparticles with polyelectrolyte[67]. Using EPD method to fabricate organic-inorganic composite materials is a fast and economic way because of the feasibility of combining the properties of each component. In this case, it is a promising and incomparable way to use polyelectrolytes for EPD method to fabricate advanced organic-inorganic composite coating. The advantage is that co-deposition of organic and inorganic materials can be achieved under room temperature processing to avoid problems such as shrinkage and cracks. The structure, properties and morphology of the composite films can be tailored according to specific requirements for various applications. This can be obtained by variation of bath composition, deposition parameters such as deposition time, deposition voltage, deposit concentration and mass transport conditions for organic and inorganic materials[19]. Different thickness and composition of coating can be easily achieved by changing the conditions of EPD deposition parameters.

In addition to polyelectrolytes, polymer-metal ion complexes provide another approach to form composites. Metal ions can attach to the polymer ligand and form a coordinate bond between each other and form chelation[19]. This promising approach could be utilized in material chemistry area such as self-assembly and synthesis nanoparticle.

2.8.1 EPD of strong polyelectrolytes and inorganic particles

The deposition of the composite film relies on the interactions of polyelectrolytes and inorganic nanoparticles at the electrode surface. To successfully fabricate composite material, suspensions need to be stable and well dispersed. Particles must coagulate at the electrode surface to form a film [32].

The charge compensation mechanism is critical for the fabrication of organic-inorganic nanocomposites. For instance, poly(diallyldimethylammonium chloride) (PDDA) can be used in EPD to fabricate organic-inorganic composites[58]. PDDA is positively charged which could be used in cathodic deposition. Investigations failed to achieve pure PDDA deposits because of the strong electrostatic repulsion of PDDA, but co-deposition of PDDA and the ceramic particles was successfully achieved [68]. Deposit formation results from columbic attraction between two oppositely charged species: positively charged PDDA and negatively charged ceramic particles which are formed at the electrode surface[4]. Besides, hydrogen bonding and ion-dipole interactions also promote the deposit formation on the electrode surface. These interactions are important for deposits and microstructure formation.

It was proved that the properties of the composites can be varied by the variation of PDDA concentration in suspension. The co-deposition of PDDA and ceramic particles is critical for the fabrication of thick coating by EPD method. The PDDA also works as a binder which provides efficient binding properties and preventing cracking. In addition, the negatively charge of inorganic nanoparticles can be compensated by the positively charged PDDA to reduce the electrostatic repulsion on the substrate surface.

2.8.2 EPD of weak polyelectrolytes and inorganic particles

Weak polyelectrolyte can prevent the nanoparticles to aggregate and maintain them well-dispersed. One critical properties of weak polyelectrolytes is that the charge of them will reduce with the pH change. For example, positively charged polyelectrolyte poly(ethylene imine) (PEI), shows a decreasing charge and can be deposited on the cathode surface due to the local surface pH increase. In addition, composite films can be obtained when combining electrosynthesis of inorganic particles with EPD of polyelectrolytes.

The EPD of PEI-Mn complex has been used for the deposition of nanocomposites with Mn_3O_4 particles[69]. The deposition mechanism is widely studied. It is proposed that PEI acquires a positive charge because of complex formation with metal ions such as Mn^{2+}.

Under the influence of the electric field, the polymer-metal ion complexes accumulate on the electrode. These polymer-metal ion complexes participate in cathodic reactions to form nanoparticles of metal oxides. This method provides advantages for the manufacture of electrode materials for supercapacitor devices. In addition, Hasegawa et al. have concentrated on the use of PEI for the surface charging of silica nanoparticles and deposition of composites by EPD method[67].

Both polyelectrolytes and inorganic nanoparticles can be electrophoretically deposited to form organic-inorganic composites. By changing the pH value of the suspension, the charge and solubility of the polyelectrolyte can be easily controlled. As a weak polyelectrolyte, chitosan (CHIT) could be cathodically deposited because of its pH-dependent charge and solubility properties[70, 71]. CHIT is soluble when it is protonated. And when neutralized, CHIT can be deposited at the cathode to form a film, as shown in Eq.2-15:

$$\mathrm{CHIT - H^+ + OH^- \rightarrow CHIT + H_2O} \tag{2-15}$$

Several studies focus on the electrophoretic codeposition of CHIT and inorganic or organic nanoparticles. It was demonstrated that CHIT promotes the EPD and the latex nanoparticles can be uniformly distributed in the CHIT film[72].

Recently the manufacture of CHIT-hydroxyapatite (HA) composite coating by EPD method has been proved[73]. It was shown that CHIT-HA composite films provided good corrosion protection of substrate in the simulated body fluid solutions. This method proves that room temperature fabrication of the composite coatings can be achieved by EPD method. In this case, the problems related to the sintering of HA deposits could be avoided.

2.9 Binder

Ceramic particles EPD has the advantage of forming uniform ceramic films with good dense packing. However, the use of fine particles induces cracking in deposited films. So in order to obtain crack-free and compact deposits, a binder is frequently introduced because it may enhance the effect of the van der Waals' force. As a result, the adherence and film strength can be increased. The optimal amount of binder added into the suspension is variable and is determined by the particle surface area and particle size.

Long-chain polymers are widely used in EPD to act as a binder. Besides, metal alkoxides and hydroxides have also been used as binders. A variety of binders have been utilized in colloid processing such as alkyd resin[74], polyvinyl-pyrrolidone[54] and polyvinyl butyral[75]. It is preferable to apply the binders, which also work as a dispersing agent to disperse different materials. Many studies show that various dispersant aids with a natural binding effect. However, limited water-soluble binders can be used comparing with non-aqueous suspension. The low adhesion strength greatly restricts their effect. There are two ways to make polymer deposits. Positively charged ceramic particles offer electrophoretic transport of the polymeric macromolecules, which are electrically neutral and adsorb onto the surfaces of the ceramic particles. The film formation mechanism is shown in Figure 2-13(a). Another way is that some cationic polyelectrolytes has good binding properties, thus they could be utilized for particle charging and EPD. The mechanism is shown in Figure 2-13(b)[4].

Binder plays an important role in the EPD method. Polymer binders are applied to achieve uniform deposit with good adherence and low cracks. Besides, polymer can offer efficiently steric stabilization to disperse nanoparticles and reduce suspension viscosity to increase deposit rate. In EPD process, charged particles can carry adsorbed polymers, move together to the electrode and deposit on surface. This process allows the polymer binders to be included in the deposits.

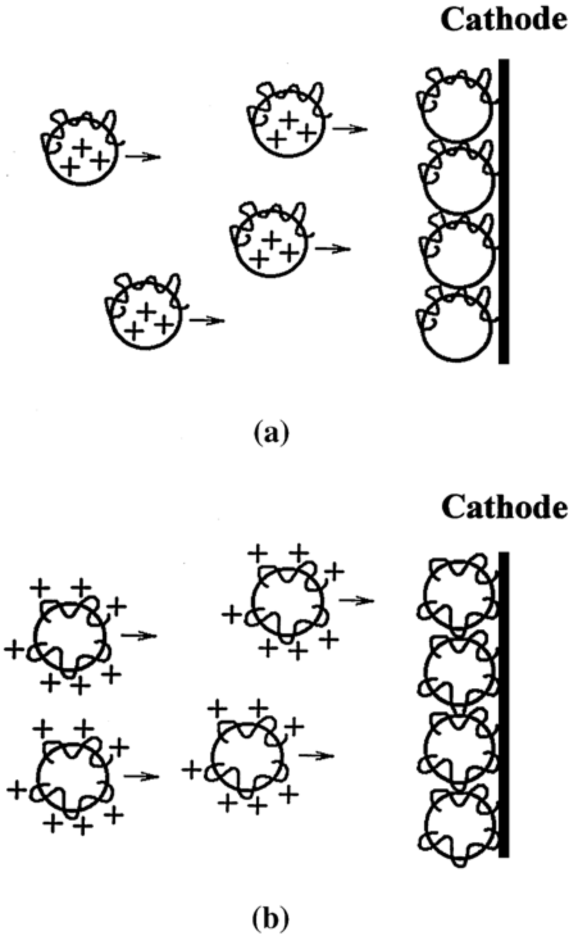

Figure 2-13 Cathodic electrophoretic deposition of ceramic particles with adsorbed (a) neutral and (b) charged polymers[4]

3. Objective

Despite the impressive progress achieved in the development of EPD method, there is a need for simple and versatile techniques for the efficient dispersion and charging of various materials to the fabrication of organic-inorganic composite films.

Therefore, my research mainly focus on three parts:

(1) Develop advanced dispersing agents with new adsorption mechanism on inorganic particles.

(2) Investigate universal dispersing agents for the colloidal processing to disperse metal, oxide, nitride, macromolecules and CNTs.

(3) Using advanced colloidal processing to fabricate organic-inorganic composite coating and other functional materials for various applications.

4. Experimental Procedures

4.1 Materials

The materials listed in the following Table 4-1 were purchased from industrial suppliers and were used for the fabrication of organic-inorganic composites.

Table 4-1 Materials purchased from commercial suppliers

Category	Material	Supplier
Metal oxide	Titanium dioxide (TiO_2)	Sigma-Aldrich
Nitride	Titanium nitride (TiN)	Alpha Products Morton Thiokol Inc.
	Silicon nitride (Si_3N_4)	H.C. Starck
Metal	Palladium (Pd)	Alfa Aesar
Electrolyte	Sodium sulfate (Na_2SO_4)	Sigma Aldrich

	Sodium chloride (NaCl)	Sigma Aldrich
Minerals	Aluminum- magnesium- zirconium hydroxide (XZO)	MEL Chemicals
	Huntite ($Mg_3Ca(CO_3)_4$)	Sibelco
	Zirconia (TZ-12CE)	Tosoh
	Hydrotalcite ($Mg_6Al_2CO_3(OH)_{16}\cdot 4(H_2O)$)	Sigma-Aldrich
	Alumina platelets	Elf Atochem
	Aluminiumhydroxide	Sigma-Aldrich
Conductive carbon materials	Multiwall carbon nanotubes (MWCNTs)	Arkema
	Graphite	Fisher Scientific
	sodium alginate	Sigma-Aldrich

Dispersing/ film forming agent	sodium hyaluronate	Sigma-Aldrich
	MaterialsPoly[1-[4-(3-carboxy-4-hydroxyphenylazo)benzenesulfonamido]-1,2-ethanediyl, sodium salt] (PAZO)	Sigma-Aldrich
	Celestine blue dye (CB)	Sigma-Aldrich
	Chitosan (CHIT)	Sigma-Aldrich
	Poly(styrene-alt-maleic acid) sodium salt solution (PSMA)	Sigma-Aldrich
	Lauryl gallate (LG)	Sigma-Aldrich
	Tannic acid (TA)	Sigma-Aldrich
Other chemicals	Potassium permanganate ($KMnO_4$)	Sigma Aldrich
	Poly(4-vinylpyridine-co-butyl methacrylate (PVB)	Aldrich Chemical

	Sodium hydroxide (NaOH)	Sigma Aldrich
	Polyvinylpyrrolidone (PVP)	Alfa Aesar
	Ethanol	Greenfield Alcohol Inc
	Acetic acid (CH_3COOH)	Caledon
	Sulfuric acid (H_2SO_4)	Caledon
	Sodium nitride ($NaNO_3$)	Caledon
	Hydrogen peroxide (H_2O_2)	Fisher Scientific
	Polyetheretherketone（PEEK）	Victrex
Current collector	304 stainless steel foils	Alfa Aesar
	Nickel foam (porosity ~95%)	Vale
	Graphene coated nickel foam	CVD Equipment Corporation

4.2 Electrophoretic Deposition Methodology

Electrophoretic deposition was performed on 304 grade stainless steel foil substrates. The substrates were polished and then cleaned with distilled water and ethanol. The size of the substrates and platinum (Pt) counter electrodes was 50 x 25 x 0.1 mm. Substrates and counter electrodes were connected to an electrode holder. The distance between counter and substrate was 15 mm. The electrode holder was connected to a constant voltage power supply. Electrodes were then submerged into suspensions, which were ultra-sonicated or stirred for at least 15 minutes before deposition. Applied voltage for depositions ranged from 5-130V and deposition time varied from 30s to 5min.

All the coatings were prepared using fresh solutions. The coatings obtained were dried in air at room temperature for at least 24 hours before the further characterization.

4.3 Investigation of deposit mass

The mass of deposit was investigated by measuring the weight of the substrates before and after deposition. In this study, Mettler Toledo AX105 DeltaRange analytical balance was used. The accuracy of balance is 0.01 mg. A minimum of 3 samples were prepared in each deposition investigation. The deposition yield measurements were repeatable and the error was less than 5%.

4.4 Material synthesis

In this research, MnO_2 nanoparticles were prepared by reduction of $KMnO_4$ using ethanol (Eq.4.1).

$$4MnO_4^- + 3CH_3CH_2OH \rightarrow 4MnO_2 + 3CH_3COO^- + OH^- + 4H_2O \qquad (4\text{-}1)$$

0.33g $KMnO_4$ was added into 100 mL deionized water and stirred for 1 hour to form homogeneous $KMnO_4$ solution. Then 50 ml ethanol were added into $KMnO_4$ solution, which was ultra-sonicated for 1 hour and then under stirred for 24 hours. The black precipitate was collected using filtration and washed using 2 L water and 0.5 L dehydrated ethanol to remove ions and organics. The final powder was further dried in air for 48 hours and stored in a desiccator. The MnO_2 nanoparticles obtained using this method had a diameters varying from 30 to 60 nm[76].

The interest in application of MnO_2 for supercapacitor is attributed to high theoretical specific capacitance (1370 F g^{-1} [77-79]) of this material. The charge-discharge mechanism of MnO_2 is given by the reaction[77]:

$$MnO_2 + C^+ + e^- \leftrightarrow MnO_2C \qquad (4\text{-}2)$$

where $C^+ = H^+, Na^+, K^+$. Small particle size and electrode porosity are important for good access of the electrolyte ions (C^+) to the capacitive MnO_2 material. However, the electronic conductivity of MnO_2 is low. In order to solve this problem, MnO_2 must be mixed additives which has good conductivity and low chemical activity, such as MWCNT[78, 80, 81]. The success of MnO_2-MWCNT supercapacitor technology will depend largely on the progress in the fabrication of advanced composites, containing well dispersed MWCNT and non-agglomerated MnO_2 nanoparticles.

4.4 Material characterization

The morphology of films was tested by Scanning Electron Microscope (SEM) (JSM-7000F, JOEL, JAPAN). Samples were cut from substrate to small pieces and attached to sample holder using a copper tape. Conductive silver or nickel paste were used to connect the samples and sample holder. Finally, a 5 nm platinum film was deposited on samples. Electron microscopy studies were also performed using a transmission electron microscope (JEOL JEM 1200 EX TEMSCAN).

Deposited material was removed from the stainless steel substrate for the further tests. Composition of materials and phase were analyzed using X-ray diffraction analysis (XRD) (diffractometer Bruker D8, UK) with Cu-Kα radiation at a scanning rate of 5^{o}/min. Thermogravimetric (TGA) and differential thermal analysis (DTA) were performed using the thermoanalyzer NETZSCH STA-409, Canada. Testing was carried out on 10 mg of material inside an aluminum oxide crucible exposed to air. The heating rate of 5^{o}C/min was applied from room temperature to 1000^{o}C. Fourier Transform Infrared Spectroscopy (FTS-40 Bio-Rad, Canada) and Ultra-violet Visible spectroscopy (UV-Vis) (Agilent Technologies, spectrometer Cary-50)) were used to investigate and identify the specific functional group of organic-inorganic composites.

4.5 Electrochemical analysis

Potentiostat (Parstat 2273, Princeton Applied Research) was used to test electrochemical properties of the deposited coatings or bulk electrodes, prepared by the colloidal methods.

The counter electrode was a platinum gauze, and the reference electrode was a standard calomel electrode (SCE). Electrochemical studies were performed using a standard three-electrode cell. Surface area of the working electrode was 1 cm^2.

Potentiodynamic testing is an efficient method to study corrosion protection. In this method, Tafel plots reflect the potential and current density when corrosion occurring. These values are used to compare materials' corrosion properties. It is clearly shown on the Tafel plot which material prevents corrosion better and how the corrosion proceeds as potential increasing. The electrolyte used for testing is 3 wt% NaCl aqueous solution.

Cyclic Voltammetry and Electrochemical Impedance Spectroscopy were used to study the capacitance and impedance of supercapacitor electrodes. These values were used to compare electrochemical and energy storage properties. The electrodes were obtained by the slurry impregnation method. The slurries were used for the impregnation of Ni foam current collectors. The impregnated current collectors were dried in air and then pressed to 30% of original thickness. The mass loading of the impregnated material was 30 mg cm^{-2}. The electrolyte used for testing is 0.5M Na_2SO_4 aqueous solution.

CV study was performed within a potential range of 0 to 0.9 V versus SCE for testing MnO_2-CNT composite. Scan rate varies from 2mv/s to 100mv/s. EIS study was performed within a frequency range from 0.01Hz to 100 kHz. The complex AC capacitance $C^*=C'-jC''$ was obtained from the impedance data[82].

5. Universal dispersing agent – PAZO

5.1 Motivation and origin

Dispersing agents typically show adsorption on limited number of materials of specific groups, such as specific metal oxides. However, the development of composites requires the use of efficient co-dispersants for all the individual components. Therefore, there is a need to develop a universal dispersing agent to disperse and deposit many kinds of inorganic and organic materials.

Poly[1-[4-(3-carboxy-4-hydroxyphenylazo)benzenesulfonamido]-1,2-ethanediyl, sodium salt] (PAZO) polyelectrolyte exhibits a unique set of properties, allowing for its diverse application in photonics, optoelectronics, memory devices[83-85]. A significant amount of research was focused on the analysis of optical storage and photochromic properties, surface-relief grating[86-89]. Our interest in PAZO is related to the significant benefits for application in EPD. The unique properties of the PAZO is that each monomer of PAZO includes diaromatic monomers with salicylate ligands. The chelating salicylate ligands of the PAZO monomers can create multiple adsorption sites on surfaces of inorganic particles. Such monomers can provide multiple adsorption sites for efficient adsorption on particles of various materials and impart electrical charges to the particles. Moreover, PAZO is a long chain structure polymer, which offers the efficient electrosteric stabilization. Therefore, the long hydrocarbon chain of PAZO and the adsorbed PAZO macromolecules, containing monomers with anionic COO^- groups, allowed for much stronger adsorption compared to the small salicylate family molecules which only contain a single salicylate ligand[37]. The structure and adsorption mechanism of PAZO is shown in Fig 5-1.

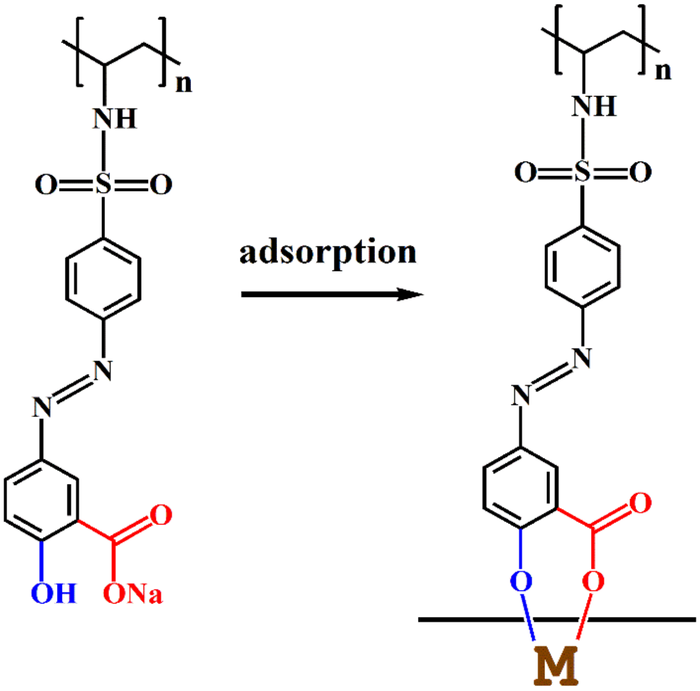

Figure 5-1 Structure and adsorption mechanism of PAZO, involving complexation of salicylate ligands with metal atom (M) on the particle surface

The goal of our investigation was to develop a universal dispersing agent for the fabrication of organic-inorganic nanocomposite. A conceptually new approach developed in this investigation utilized physical properties of PAZO and various functional materials. We demonstrate that various functional materials of different types and composition can be deposited using PAZO as a dispersing, charging and film forming agent. This versatility is a unique feature of PAZO comparing to traditional dispersing agents which are only capable of dispersing a few specific materials for EPD. The results of this investigation pave the way for the deposition of composite films utilizing different materials and PAZO.

5.2 Film formation properties

EPD offers significant advantages for the deposition of PAZO films due to the simple deposition procedure, high deposition rate, possibility of deposition of thin and thick films. Moreover, EPD allows for the deposition of pure PAZO films as well as composites at controlled deposition rate, containing functional inorganic materials in the PAZO matrix. The composition can be varied by variation of concentration of inorganic particles in the PAZO solutions. Traditionally, layer-by-layer (LbL) self-assembly technique has been utilized for the fabrication of functional films, containing PAZO[90]. However, the LbL method requires multiple and time consuming steps[91-93]. The need for faster processes has driven the study based on EPD method. In this investigation the EPD of PAZO films and composite films has been studied.

The film formation mechanisms are well described in the literature[94]. It was found that anodic films can be obtained from 0.05-1.0 g L^{-1} PAZO solutions in methanol or ethanol-water solvent[94]. The deposition mechanism involved the electrophoresis of negatively charged PAZO macromolecules toward the anode and accumulation at the anodic substrate. The electrochemical decomposition of methanol[83] or water[84] in anodic reactions resulted in H^+ generation and the charge neutralization of COO^- groups, which promoted deposit formation of PAZO. Such properties can be utilized for film formation by EPD.

In aqueous solutions, the electrochemical decomposition of water results in a pH decrease at the anode surface:

$$2H_2O \rightarrow O_2 + 4H^+ + 4e^- \qquad (5\text{-}1)$$

The charge neutralization of carboxylic groups of PAZO at the anode surface and formation of insoluble PAZO polymer promoted deposit formation:

$$-COO^- + H^+ \rightarrow -COOH \qquad (5\text{-}2)$$

In this investigation, a soluble sodium salt of PAZO (PAZO-Na) was used for deposition. The charge neutralization at anodic surface results in the precipitation of the insoluble acidic form of this polymer (PAZO-H). Therefore, it is suggested that the low solubility of the PAZO polymer was an important factor in the successful deposition of PAZO at the anode surface. EPD of PAZO and other materials was performed using solutions or suspensions in mixed ethanol–water (25% water) solvent. PAZO showed low solubility in ethanol. The use of mixed solvent offered the advantage of reduced gas evolution at the electrode surface during EPD. The film forming and binding properties of PAZO offered additional benefits for EPD to fabricate adherent films.

Fig 5-2 shows SEM images of the PAZO films prepared by EPD method from 1 g L^{-1} PAZO solutions. The PAZO films were continuous and crack free. The film porosity can result from gas evolution during deposition or solvent evaporation during drying.

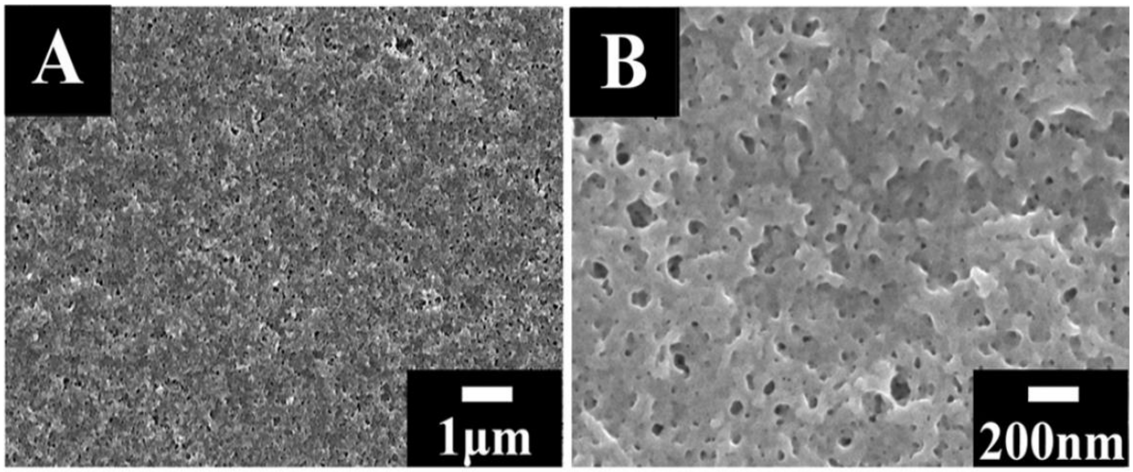

Figure 5-2 SEM images of films, prepared from 1 g L^{-1} PAZO solutions in ethanol–water solvent at a deposition voltage of 10 V and deposition time of 3 min

5.2 Dispersion and deposition of inorganic materials

The use of PAZO as a dispersing, charging and film forming agent allowed the EPD of various materials such as metals, metal oxides, nitrides, carbides, polymers and minerals. It is expected that PAZO can be used for EPD to fabricate novel composites, utilizing functional properties of different materials and unique physical properties of PAZO[95].

Previous investigations[37] of small molecules from the salicylic acid family showed their adsorption on inorganic particles, such as TiO_2. Adsorption mechanisms included bidentate chelating bonding or bidentate bridging bonding, which involved the salicylate ligands of the molecules and metal atoms on the particle surface. The use of aromatic molecules, containing salicylate ligands, allowed for their application as co-dispersants for inorganic particles and carbon nanotubes. The $\pi - \pi$ interactions promoted adsorption on carbon nanotubes, whereas the salicylate ligands created bonds with the metal atoms on the particle surface. This approach has had limited applications due to relatively weak interactions of single salicylate ligands of the small molecules with the particle surfaces.

In our investigation, the unique adsorption and film forming properties of PAZO allowed for the dispersion and EPD of various materials. We demonstrate that various functional materials of different types, such as TiO_2, zirconia, TiN, Si_3N_4, Pd metal, SiC and carbon nanotubes can be deposited by PAZO. This versatility is a unique feature of PAZO and addresses the limitation of other traditional dispersing agents, that they are only capable of dispersing a few specific materials for EPD. The results of this investigation pave the way for the deposition of organic-inorganic composites utilizing the functional properties of different materials and PAZO.

The deposition yield was studied for the films deposited on stainless steel substrates. Due to limitations of the concept of zeta-potential for the analysis of the electrokinetic behavior of particles, containing adsorbed polyelectrolytes, the deposition process was analyzed using the deposition yield data. The deposition yield in the EPD process depends on various parameters, such as deposition time, concentration of particles, particle size, and concentration of dispersant, chemical properties of particles, composition of solvent and other factors. We present the deposition yield data for different materials at selected deposition voltage of 100 V and deposition time of 4 min in a mixed ethanol–water (25% water) solvent for PAZO concentrations in the range of 0–1 g L^{-1}.

We found that the increase in PAZO concentration in the suspensions resulted in increasing adsorption of PAZO on the particles of metal oxides and nitrides, and therefore increasing particle charge and mobility. As a result, we observed the increase in deposition yield with increasing PAZO concentration in the range of low concentrations (Fig 5-3).

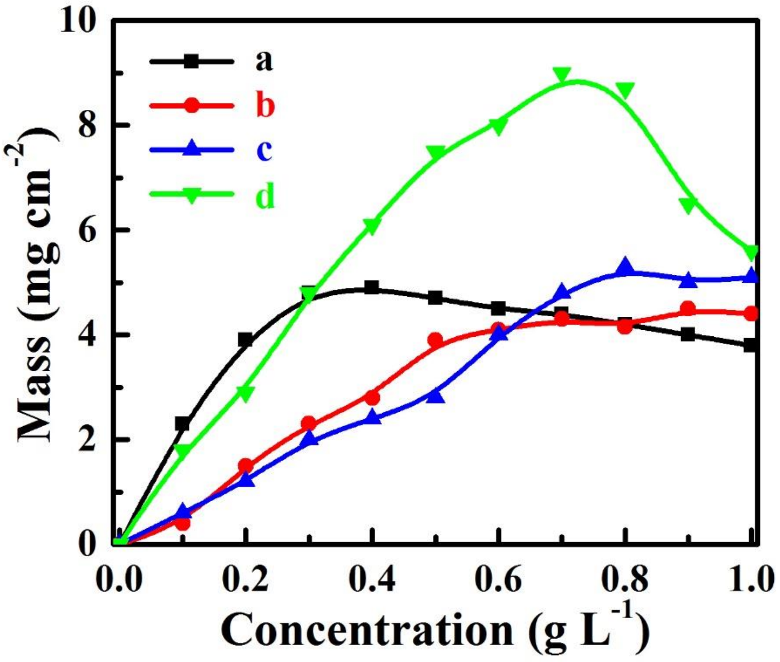

Figure 5-3 Deposit mass versus PAZO concentration in suspensions, containing 4 g L^{-1} of (a) TiO_2, (b) zirconia, (c) TiN, (d) Si_3N_4 at a deposition voltage of 100 V and deposition time of 4 min

The deposition yield of TiO_2 and Si_3N_4 increased with increasing PAZO concentration and showed maximum deposit mass. The deposition yield of zirconia and TiN increased with the increasing PAZO concentration. The deposition yield versus PAZO concentration dependences allowed the optimal PAZO concentration for each material to be determined for selected deposition conditions.

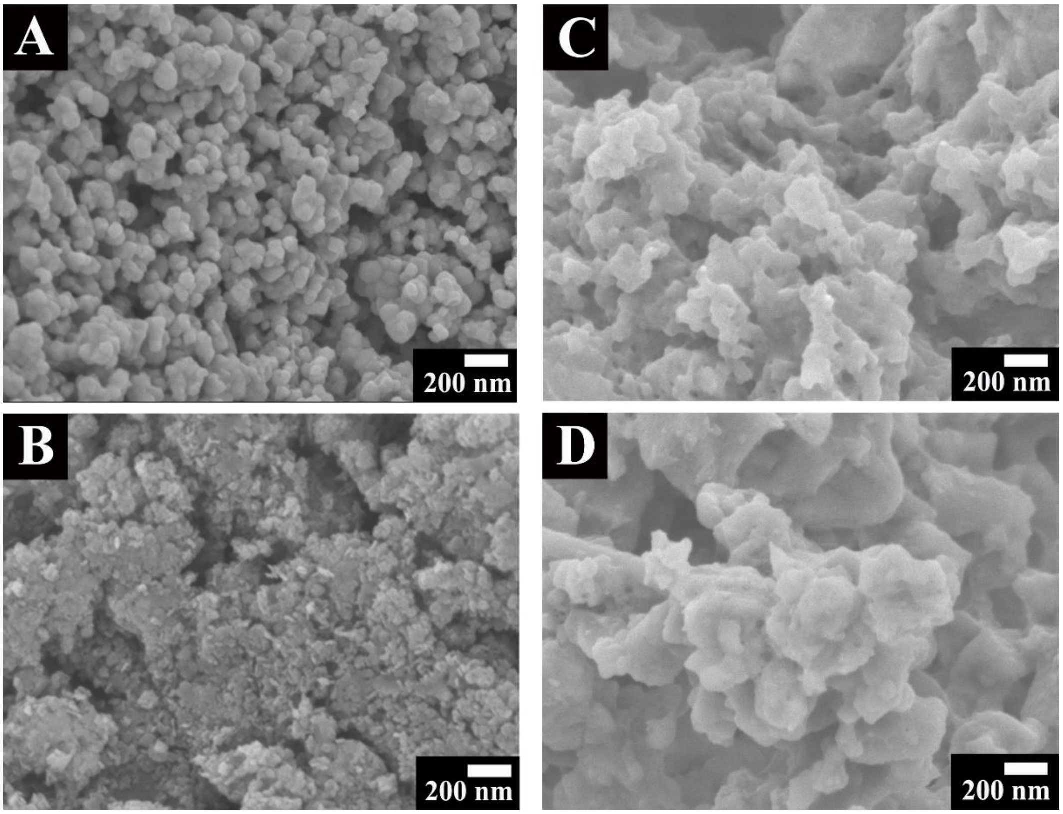

Figure 5-4 SEM images of deposits, prepared from 4 g L^{-1} suspensions of (A) TiO_2, (B) zirconia, (C) TiN, (D) Si_3N_4 in a mixed ethanol–water solvent, containing 1 g L^{-1} PAZO

The SEM images of deposits formed from 4 g L^{-1} suspensions of the metal oxides or nitrides, containing 1 g L^{-1} PAZO are shown in Fig 5-4. Deposition from these relatively concentrated suspensions resulted in porous films. The film porosity was the result of particle packing, with the pores comparable in size to the deposited particles.

Fig 5-5 shows deposit mass versus PAZO concentration in the suspensions of other organic and inorganic materials, such as MWCNT, Pd metal particles and SiC. The deposition yield of MWCNT increased with increasing PAZO concentration and showed maxima or plateaus. There results allowed to optimize the concentration of PAZO for EPD application.

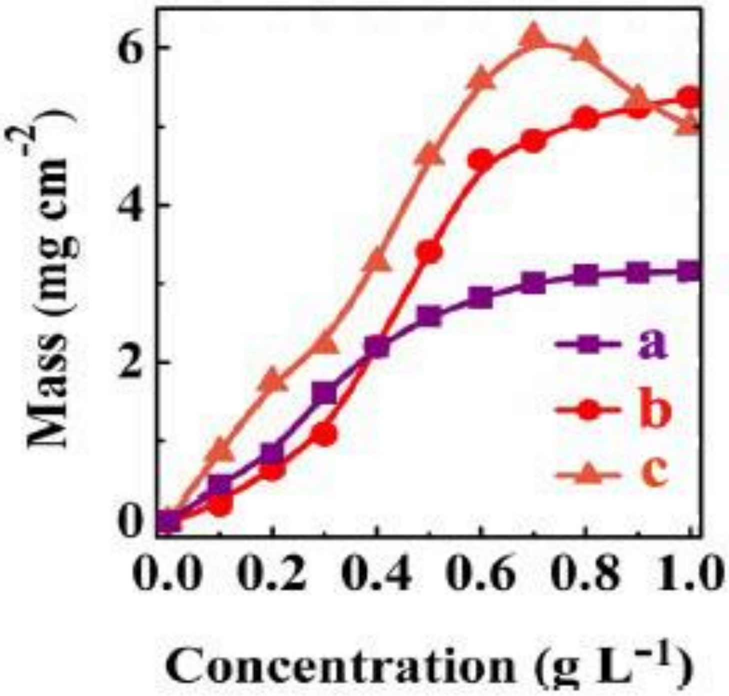

Figure 5-5 Deposit mass versus PAZO concentration in 4 g L^{-1} suspensions of (a) MWCNT, (b) Pd, (c) SiC, in a mixed ethanol–water solvent, at a deposition voltage of 100 V and deposition time of 4 min

The corresponding SEM images of the various deposits are shown in Fig 5-6 and confirm the successful deposition of MWCNT, Pd and SiC. The deposits contained a large number of particles and showed porosity with the size of the pores being comparable to the size of the particles. We found that the composition, microstructure and porosity of the deposits can be varied.

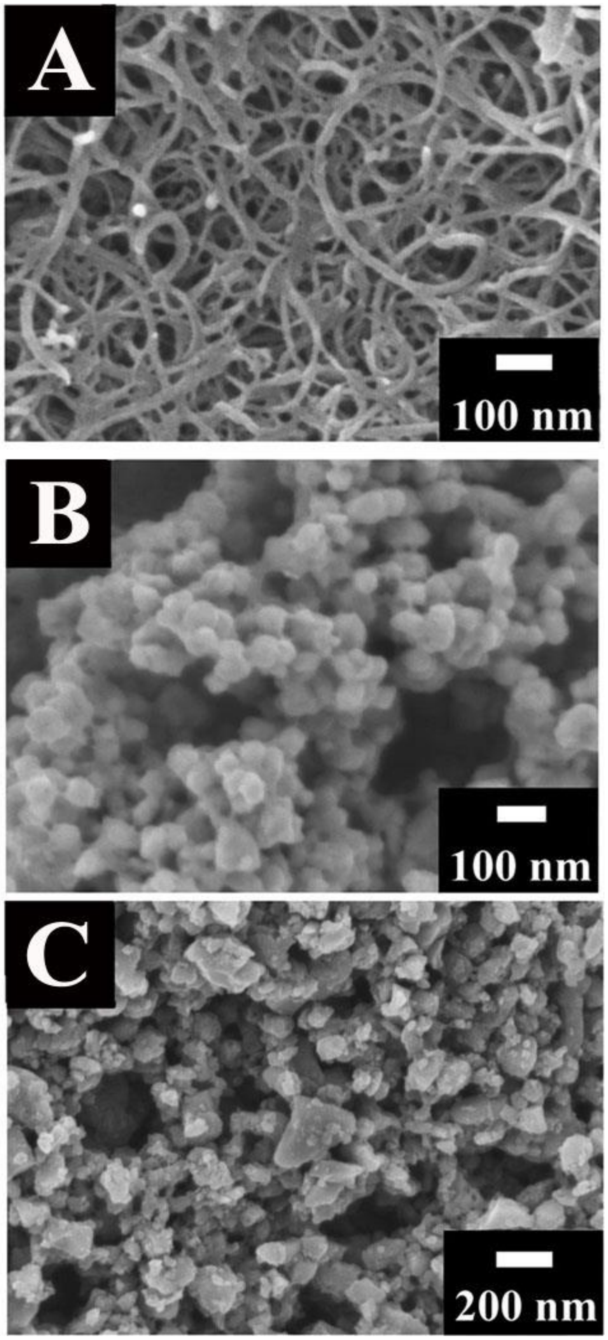

Figure 5-6 SEM images of deposits, prepared from 4 g L^{-1} suspensions of (A) MWCNT, (B) Pd, (C) SiC in a mixed ethanol–water solvent, containing 1 g L^{-1} PAZO

The results presented above indicated that PAZO showed strong adsorption on different materials. The adsorption of PAZO on different materials is of critical importance for their dispersion and EPD. It is suggested that the adsorption mechanism of PAZO on inorganic materials involves complexation of metal atoms on the particle surface with salicylate ligands of individual monomers. The adsorption of PAZO on MWCNT is governed by $\pi - \pi$ interaction and hydrophobic interactions. In contrast to small organic molecules from the salicylate family, which contain only one salicylate ligand, the salicylate ligands of individual PAZO monomers provide numerous adsorption sites. Moreover, PAZO offers benefits of enhanced electrosteric dispersion due to multiple charges of individual monomers and its large molecular size. In addition, PAZO exhibits important film forming properties. As a result, PAZO showed superior performance in the EPD of individual materials, compared to the small molecules from the salicylate family. Of particular interest is the possibility of EPD of nanoparticles of metals, carbide, nitride and MWCNT.

Fig 5-7 compares SEM images at the same magnification of pure PAZO and composite films, prepared from Si_3N_4 suspensions. A 1 g L^{-1} PAZO concentration was used and the Si_3N_4 concentration was 0-4 g L^{-1}. Films, prepared from 1 g L^{-1} PAZO solutions, containing 0–0.6 g L^{-1} Si_3N_4 were relatively dense (Fig 5-7 A – C). Increasing the particle concentration in the suspensions from 0.2 to 0.6 g L^{-1}

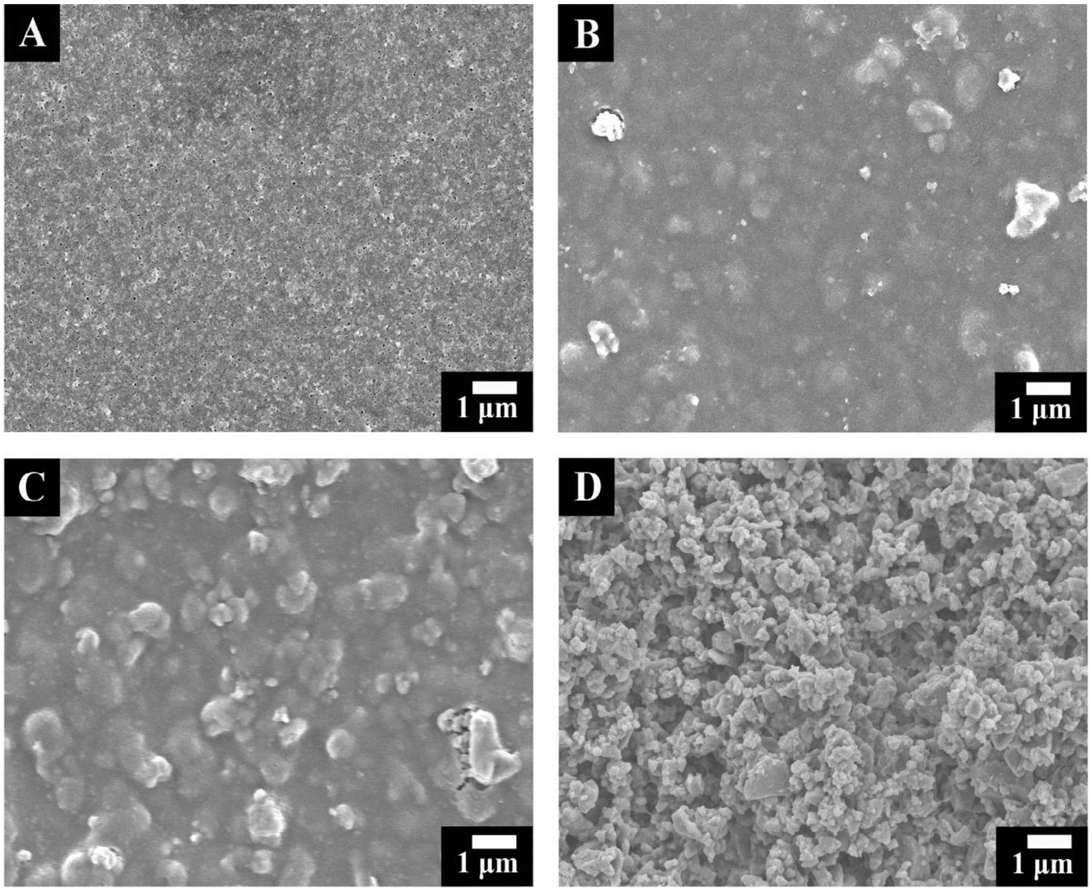

Figure 5-7 SEM images of deposits prepared from 1 g L^{-1} PAZO solutions in a mixed ethanol–water solvent: (A) without additives and containing (B) 0.2, (C) 0.6 and (D) 4 g L^{-1} Si_3N_4

resulted in increased particle concentration in the deposit. The deposit prepared from the 4 g L^{-1} Si_3N_4 suspension (Fig. 5-7 D), contained mainly Si_3N_4 and exhibited porosity. Therefore, EPD allowed for deposition of different materials and variation of their concentration in the PAZO matrix. The deposit morphology and composition could be varied by changing the particle concentration.

It was shown that PAZO can act as a universal dispersing agent to disperse and deposit materials of different types. Therefore, the Ni-NiO and $BaTiO_3$-$CoFe_2O_4$ composite films have been successfully fabricated by EPD method, using PAZO as a charging, dispersing and film forming agent. Fig 5-8 A shows X-ray diffraction patterns of the Ni–NiO composite with PAZO, prepared by EPD. The X-ray diffraction pattern shows peaks of NiO, Ni and indicates that such materials were co-deposited and formed a composite. The SEM image of a composite (Fig 5-9 A) shows particles of both materials. The X-ray diffraction pattern (Fig 5-8 B) shows peaks of $BaTiO_3$ and $CoFe_2O_4$, indicating their co-deposition and composite formation. The corresponding SEM image shows particles of both materials (Fig 5-9 B). Ni–NiO composites are important materials for various applications, such as electrodes of batteries[96], supercapacitors[97] and catalysts[98]. $BaTiO_3$–$CoFe_2O_4$ materials belong to the family of multiferroic composites, combining properties of ferroelectric $BaTiO_3$ and ferromagnetic $CoFe_2O_4$. The use of PAZO for the deposition of functional inorganic materials could result in the fabrication of a wide variety of composite films for many different applications.

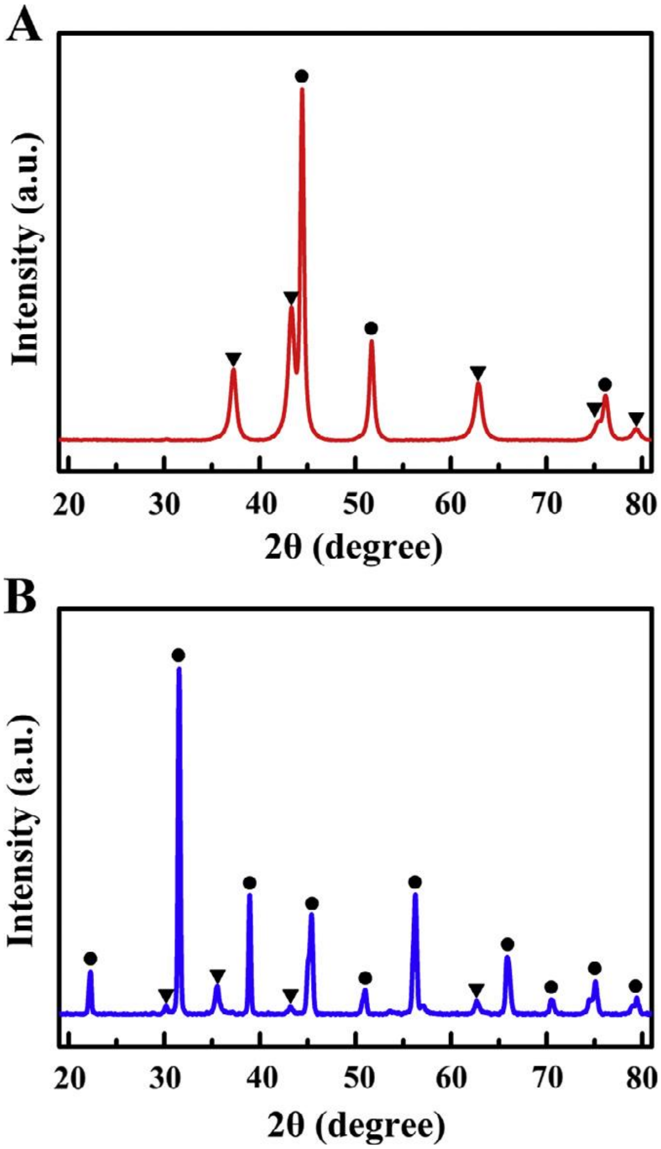

Figure 5-8 X-ray diffraction patterns of the deposits prepared from 1 g L^{-1} PAZO solutions, containing (A) 2 g L^{-1} Ni and 2 g L^{-1} NiO (● – peaks, corresponding to JCPDS file 70–1849 of Ni, ▼ – peaks, corresponding to JCPDS file 47–1049 of NiO), (B) 2 g L^{-1} $BaTiO_3$ and 2 g L^{-1} $CoFe_2O_4$ (● – peaks corresponding to JCPDS file 70–9164 of $BaTiO_3$, ▼ – peaks corresponding to JCPDS file 22–1086 of $CoFe_2O_4$)

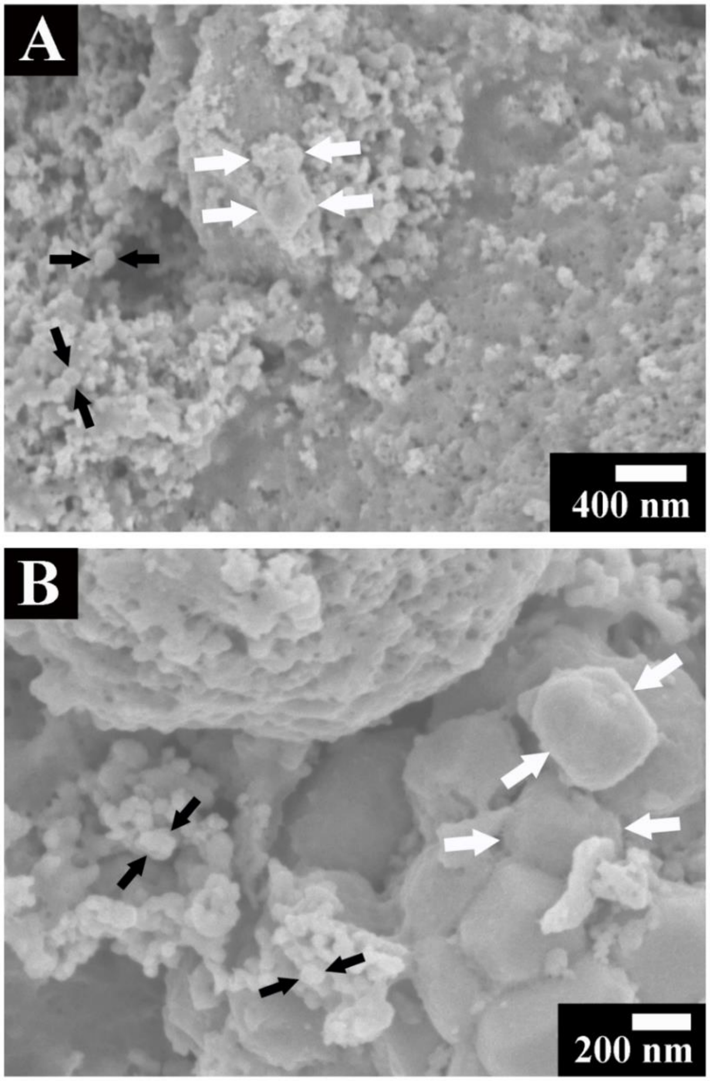

Figure 5-9 SEM images of the deposits prepared from 1 g L^{-1} PAZO solutions, containing (A) 2 g L^{-1} Ni and 2 g L^{-1} NiO (black arrows show Ni, white arrows show NiO), (B) 2 g L^{-1} $BaTiO_3$ and 2 g L^{-1} $CoFe_2O_4$ (black arrows show $CoFe_2O_4$, white arrows show $BaTiO_3$)

5.3 Dispersion and deposition of neutral polymer-mineral composites

Polyetheretherketone (PEEK) is a high performance thermoplastic material, which exhibits excellent mechanical properties. Many applications of PEEK and composites are based on the use of coatings. EPD is an important technique for the deposition of PEEK and composite coatings, but the deposited PEEK films were loose and weak in adhesion. From our investigation, some polyelectrolytes such as sodium alginate (AL) and PAZO have excellent dispersion and adsorption on related materials. Besides, the binding and film forming properties of the polyelectrolytes promoted deposit formation and the fabrication of adherent films. Thus, we use AL and PAZO to disperse PEEK large particles and successfully deposit PEEK.

AL and PAZO can be used as co-dispersants for individual components and fabrication of composite coatings. It was suggested that the adsorption mechanism of AL and PAZO on the inorganic particles involved carboxylate and salicylate type of bonding, which is shown in Fig 5-10. The adsorption of AL and PAZO on PEEK is also based on the $\pi-\pi$ interactions and hydrophobic interactions.

Fig 5-11 shows SEM images of coatings, prepared from PEEK suspensions, containing AL and PAZO polyelectrolytes. The SEM image at lower magnifications showed that the coatings were porous and contained large PEEK particles. The porosity resulted from the packing of the PEEK particles. The porosity at higher magnification showed relatively smooth thin polyelectrolyte layers on the relatively rough surface of the PEEK particles. The polyelectrolytes, adsorbed on the PEEK particle surface, provided binding of the PEEK particles.

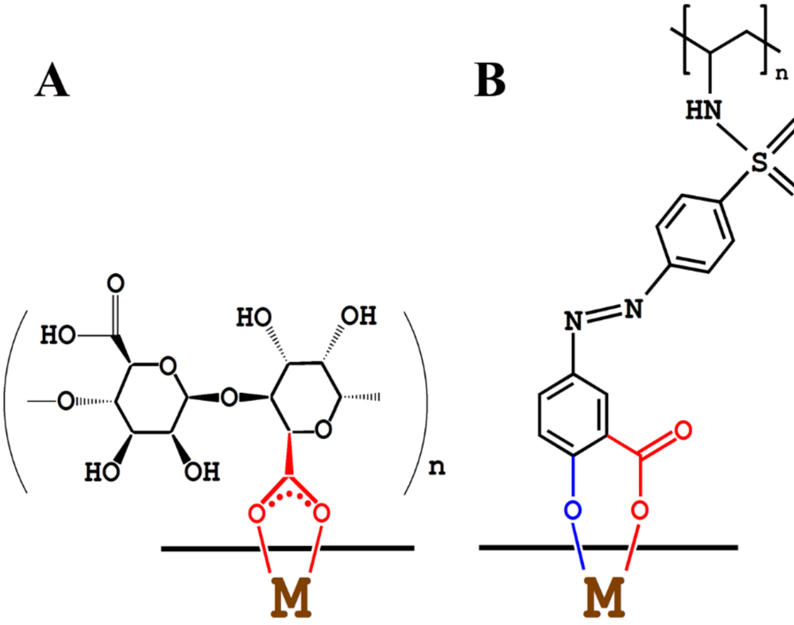

Figure 5-10 Adsorption of (A) AL and (B) PAZO, involving bonding of (A) carboxylate and (B) salicylate ligands to the metal atom (M) on the particle surface

AL and PAZO were also investigated for the dispersion and EPD of minerals such as huntite and alumina platelets. It was found that suspensions of huntite and alumina with chitosan were unstable and EPD has not been achieved from such suspensions[99]. However, the use of AL as a dispersing and charging agent allowed the deposition of huntite. AL can well disperse mineral nanoparticle, but it cannot disperse micro-size alumina platelets due to relatively poor adsorption. In contrast, anodic coatings were obtained from huntite or alumina suspensions, containing PAZO. As a result, PAZO gives strong adsorption and dispersion for both nano-sized and micron-sized mineral particles.

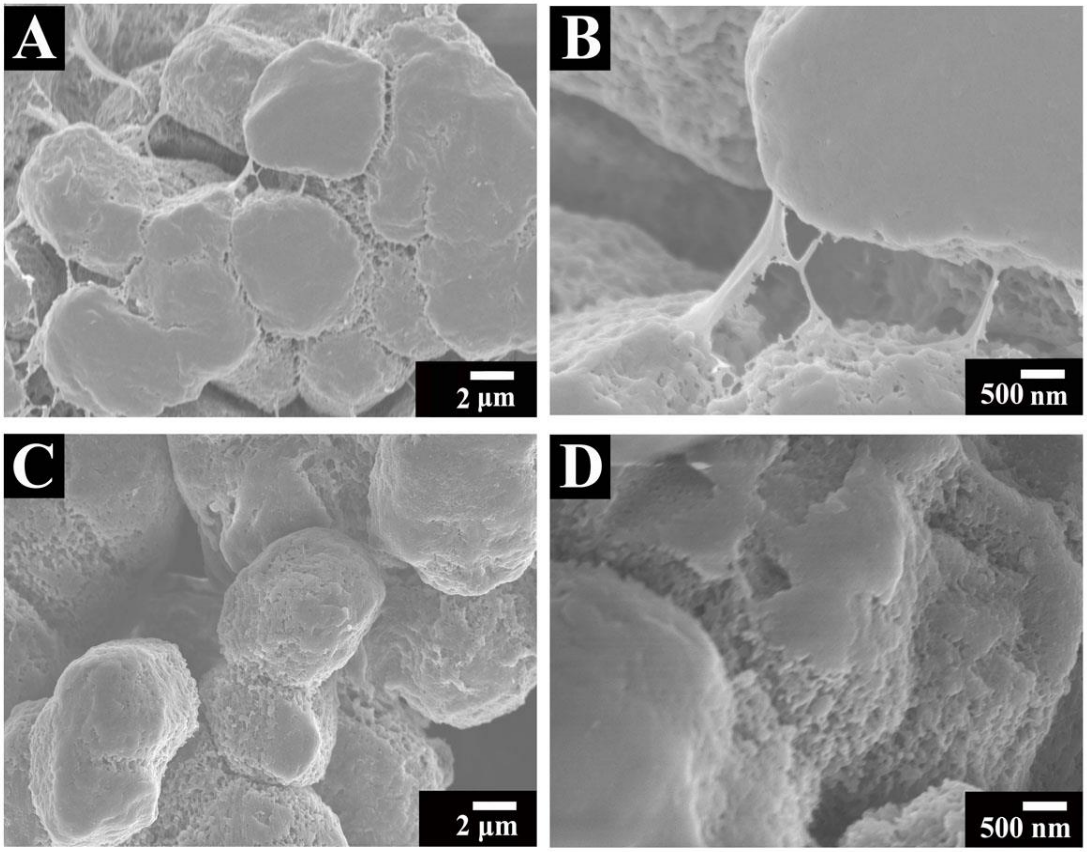

Figure 5-11 SEM at different magnifications of deposits, obtained from (A,B) 4 g L^{-1} PEEK suspension with 0.5 g L^{-1} AL and (C,D) 4 g L^{-1} PEEK suspension with 0.5 g L^{-1} PAZO at deposition voltages of 50V

Fig 5-12 shows SEM images of the huntite and alumina coatings, prepared by EPD. The images at low magnification show the formation of continuous coatings. The higher magnification images show plate-like morphology of the alumina and porosity, attributed to packing of the particles.

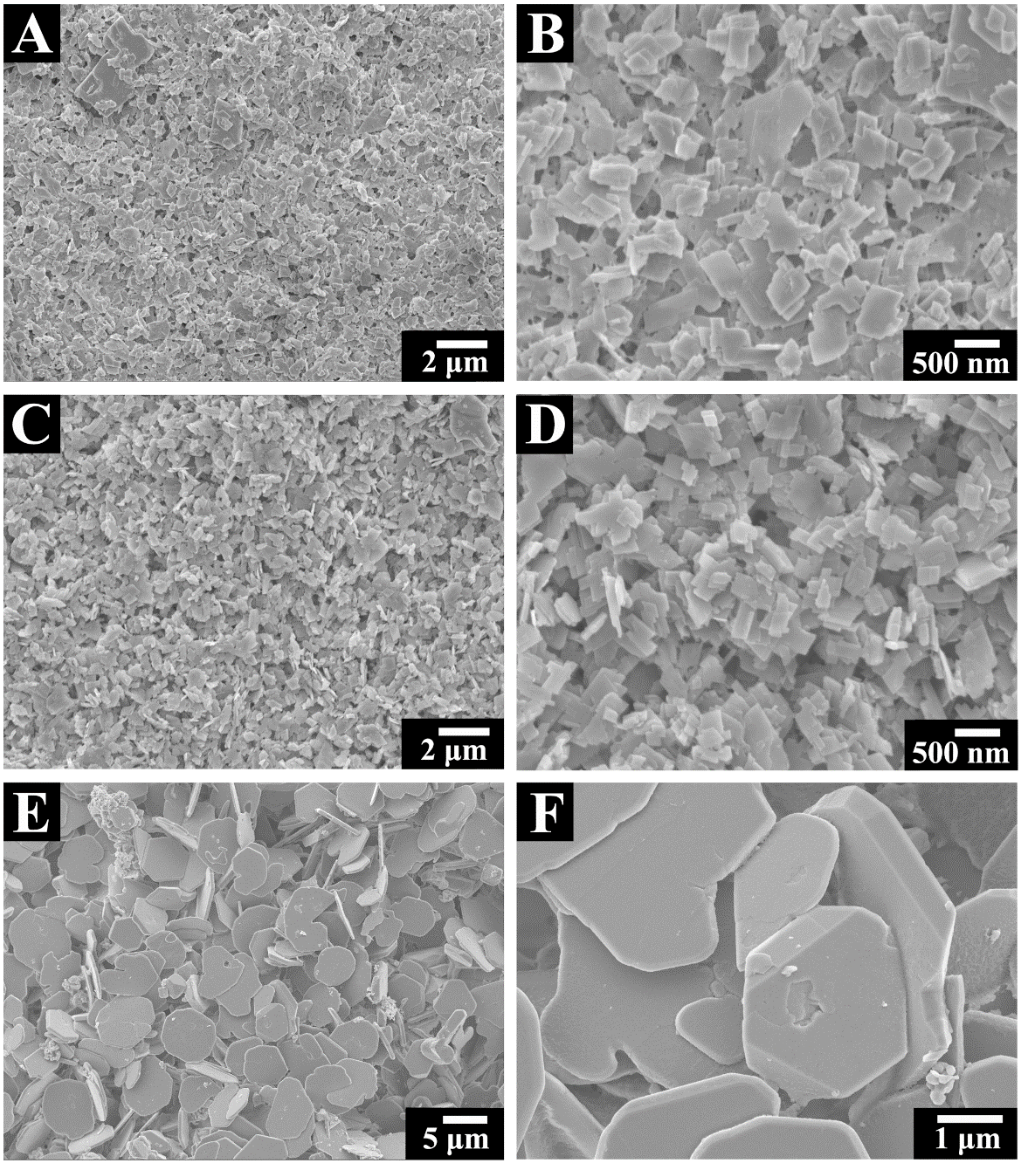

Figure 5-12 SEM images at different magnifications of deposits, obtained (A-D) using 4 g L^{-1} huntite suspension containing (A,B) 0.5 g L^{-1} AL, (C,D) 0.5 g L^{-1} PAZO and (E,F) using 4 g L^{-1} alumina suspension with 0.5 g L^{-1} PAZO at deposition voltage of 50V

Fig 5-13 shows the FTIR spectra of the deposits. This result showed characteristic absorptions[100, 101] of carbonate ligands bonded to magnesium and calcium atoms of huntite at 870 and 891 cm^{-1} and also at 1442 and 1510 cm^{-1}. The broad absorptions in the range of 1400-1600 cm^{-1} indicate contribution of the carboxylic group of AL[102] and PAZO[103], adsorbed on the huntite particles. The C-C/C=C vibrations of aromatic rings and N=N stretching vibrations[104] of PAZO contributed to the broad adsorptions in the range of 1400-1600 cm^{-1}. The bending C-H vibrations[49] of PAZO contributed to the absorptions at 1088 and 1145 cm^{-1}.The adsorption at 687 cm^{-1} is related to stretching Al-O vibrations[105]. The bands at 1488 and 1646 cm^{-1} are respectively due to symmetric and asymmetric stretching vibrations of COO$^-$ groups of PAZO. The C-C/C=C vibrations of the aromatic rings[33] of PAZO contributed to adsorptions at 1429 and 1589 cm^{-1}. Therefore, the FTIR data confirmed that deposited huntite and alumina contained adsorbed AL or PAZO polymers.

The comparison of the data for different polyelectrolytes provided an insight into the influence of cationic and anionic ligands of the polyelectrolytes on their adsorption on different particles. The chelation of COO$^-$ group of AL monomers with Mg and Ca atoms allowed for AL adsorption on huntite. The salicylate ligands of PAZO monomers, containing COO$^-$ and OH group, bonded to adjacent carbon atoms of the aromatic ring allowed for good PAZO adsorption on the Mg and Ca carbonate type huntite and alumina. Previous investigations showed superior adsorption of small aromatic molecules with salicylate ligands on various inorganic surfaces, compared to the molecules with carboxylate ligands[37]. Therefore we can expect improved adsorption of PAZO with salicylate ligands on inorganic surfaces, compared to Al with carboxylate ligands. In this case, PAZO polymer allowed for EPD of alumina platelets, whereas AL cannot be used for EPD of this material.

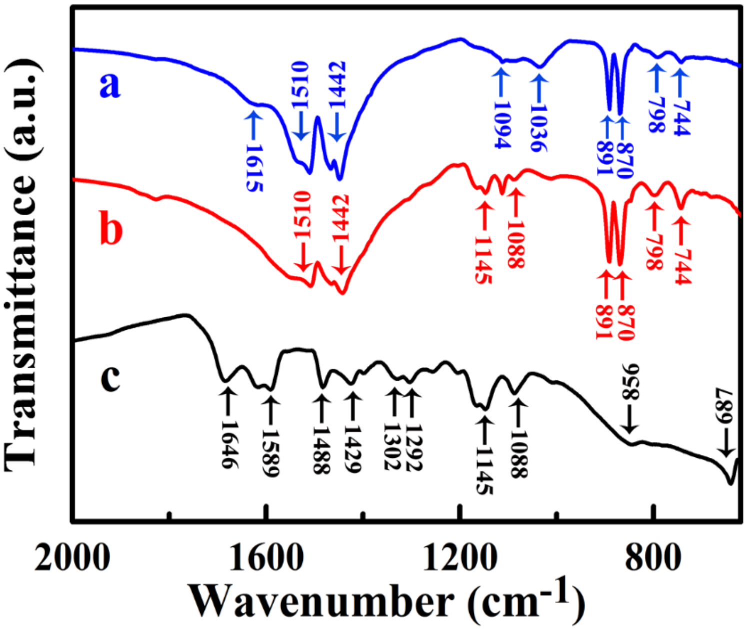

Figure 5-13 FTIR spectra of deposits, obtained (A) using 4 g L^{-1} huntite suspension with 0.5 g L^{-1} AL, (B) using 4 g L^{-1} huntite suspension with 0.5 g L^{-1} PAZO and (C) using 4 g L^{-1} alumina suspension with 0.5 g L^{-1} PAZO at a deposition voltage of 50V

Investigations showed that the charge of PEEK particles can be reversed in the presence of positively charged Al_2O_3 nanoparticles, which adsorbed on the PEEK surface. As a result, PEEK and Al_2O_3 were successfully co-deposited by cathodic EPD from suspensions in ethanol[106]. From our experiments, PEEK-huntite and PEEK-alumina composites were successfully fabricated by anodic EPD. The composite coatings after thermal processing showed improved corrosion protection of stainless steel, compared to pure PEEK coatings after thermal processing. The progress achieved in the EPD of PEEK and composites paves the way for the development of new organic coatings by EPD.

In this case, we found that PAZO can be used for EPD of PEEK based composites. The formation of the composite coating was confirmed by the results of SEM studies. The SEM images of the composite coatings (Fig 5-14) at low magnifications show relatively large PEEK particles. At higher magnification, the huntite and alumina platelets can be observed. The platelets filled the large voids between the PEEK particles. The coatings were sintered at 350°C for 30 min and their corrosion protection of the stainless steel substrates was analyzed.

Fig 5-15 shows Tafel plots for uncoated and coated stainless steel in the 3% NaCl solutions. The PEEK-huntite and PEEK-alumina coatings showed good corrosion protection, as indicated by the increasing corrosion potential and reduced corrosion current. The corrosion potentials were -389.3, -241.0, -237.8, -192.1 and -257.1 mV, the corrosion currents were 2.55, 0.76, 1.56, 2.00 and 1.56 μA cm^{-2} and corrosion rates were 26.44, 0.15, 16.17, 20.72 and 16.79 μm annually for uncoated stainless steel, PEEK-huntite coated using AL, PEEK-huntite coated using PAZO, PEEK-alumina coated using PAZO, and PEEK coated using PAZO, respectively.

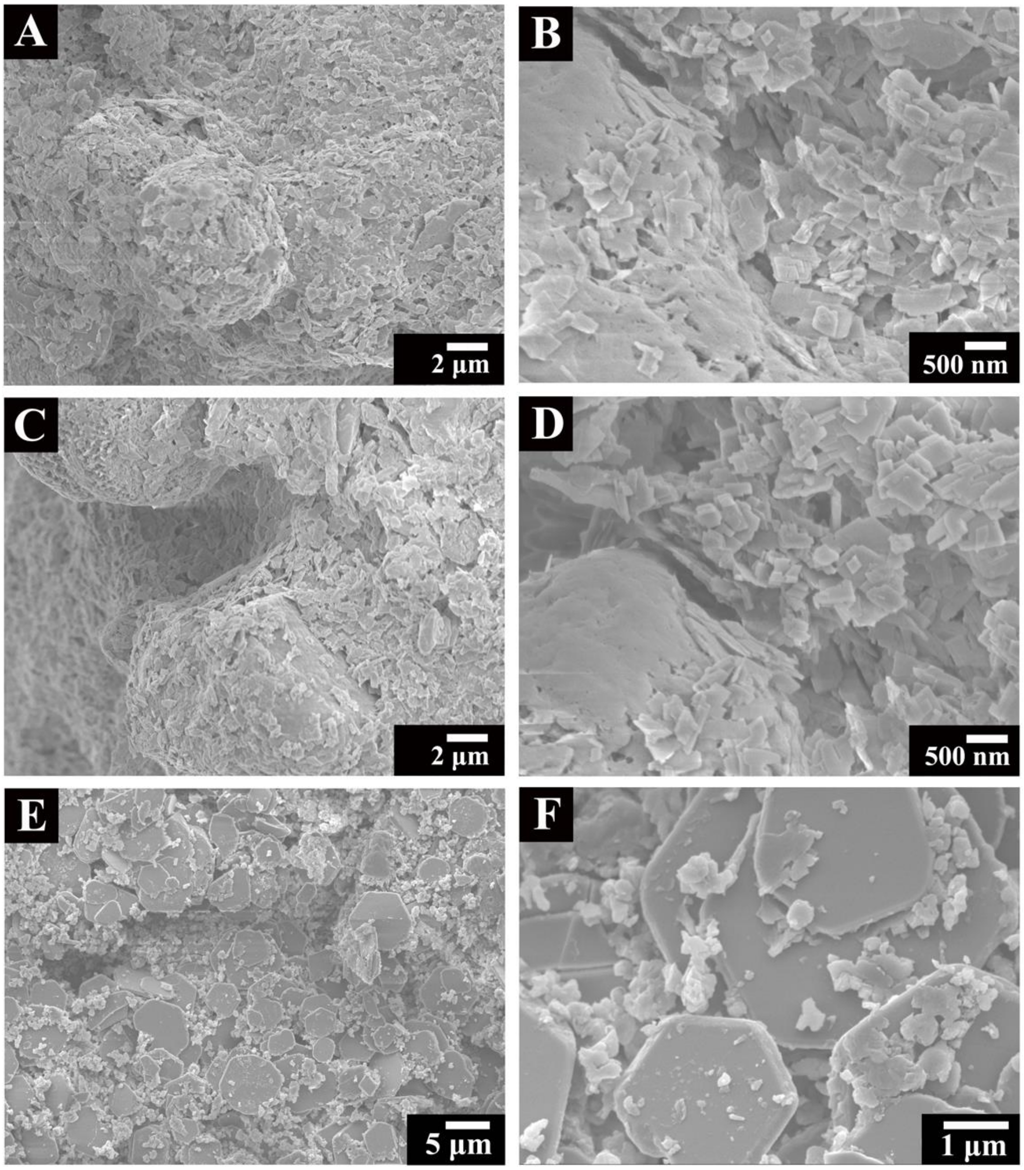

Figure 5-14 SEM image at different magnification of the EPD coatings, prepared from suspensions, containing 4g L^{-1} PEEK and (A,B) 1g L^{-1} huntite and 0.5 g L^{-1} AL, (C,D) 1 g L^{-1} huntite and 0.5 g L^{-1} PAZO, (E,F) 1 g L^{-1} alumina and 0.5 g L^{-1} PAZO

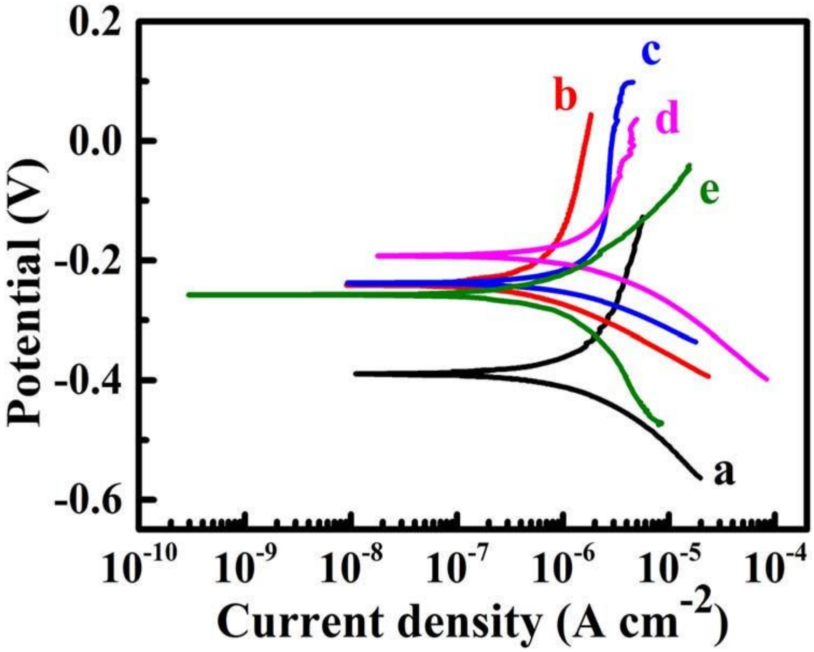

Figure 5-15 Tafel plots for (a) uncoated stainless steel, (b) coated with PEEK-huntite composite coating using AL dispersant, (c) coated with PEEK-huntite composite coating, prepared using PAZO dispersant, (d) coated with PEEK-alumina composite coating, prepared using PAZO dispersant, (e) coated with PEEK coating, prepared using PAZO dispersant

The use of Al allowed for the EPD of huntite, whereas the use of PAZO allowed for the EPD of huntite and alumina platelets. The comparison of the experimental data for the polyelectrolytes, containing monomers with different chelating ligands indicated that PAZO is a promising additive for EPD of polymers or minerals due to the strong adsorption on particle surfaces, which involves salicylate type of bonding or π - π interaction. The feasibility of EPD of PEEK coatings, containing huntite has been demonstrated. The composite PEEK-huntite and PEEK-alumina coatings provided good corrosion protection of steel.

5.4 Conclusion

The results of our investigations indicate that PAZO can be used as a universal dispersing agent for EPD of organic and inorganic materials. Films of PAZO have been deposited by anodic EPD under constant voltage conditions. The deposition yield can be varied by variation of deposition time or PAZO concentration in solutions at constant voltage conditions. The deposition mechanism involved electrophoresis of anionic PAZO macromolecules, pH decrease at the anode due to the electrode reactions, protonation of carboxylic groups of PAZO and precipitation of insoluble acidic form of PAZO. It was found that PAZO exhibits unique adsorption properties on various materials, attributed to the chelating properties of the salicylate ligands of PAZO monomers and π-π interactions. The salicylate ligands of individual monomers created multiple adsorption cites and provided adsorption on inorganic surfaces by complexation of metal atoms, and allowed for their efficient electrosteric dispersion and EPD. The properties of PAZO for application in EPD were shown by deposition of a large variety of different materials, including individual oxides, mineral, carbon nanotube, metal, nitride, carbide, and polymer. Composite films have been prepared by EPD using PAZO as a co-dispersant for different materials.

These results allowed overcoming the limitations of other dispersing agents, which can be used for specific materials only, and paved the way for application of PAZO as a universal dispersing agent for EPD of inorganic and organic materials. The versatility of PAZO as a universal charging, film-forming and dispersing agent coupled with the flexibility and control offered by EPD opens new strategies for future work on the development of specifically engineered composite films for a wide variety of important applications, utilizing optical, flame retardant additives, anti-corrosion, ferroelectric, catalytic, energy storage and other properties of PAZO and inorganic materials.

6. EPD of neutral polymers and composites using tannic acid complexes

6.1 Motivation and origin

Tannic acid (TA) is an interesting material in nanotechnology due to the unique chemical properties, which allow interactions with various metal oxides. The unique feature of TA structure is that it includes multiple galloyl groups, which promote electrostatic stabilization, hydrogen bonding, and hydrophobic interactions. The multiple galloyl groups of TA can provide multiple binding sites to form chelates with multiple particles. The chemical structure of TA is shown in Fig 6-1.

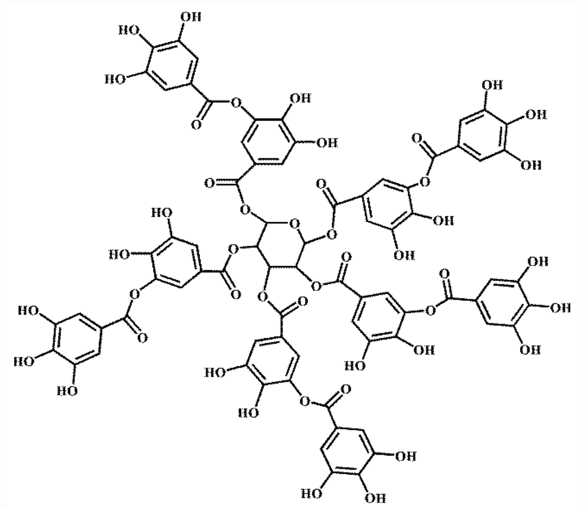

Figure 6-1 chemical structure of TA

TA showed interesting complexation behavior with various macromolecules, including carbohydrates, proteins and polymers. Also, TA was found to be an efficient dispersing agent for multiwall carbon nanotubes (MWCNT) due to the strong π - π interactions.

Moreover, TA showed interesting interactions with advanced polymers, such as polyvinylpyrrolidone (PVP). PVP is an electrically neutral polymer, containing hydrogen-accepting carbonyl groups. The chemical structure of PVP is shown in Fig 6-2. PVP can form complexes with TA through hydrogen bonding, involving the carbonyl groups of PVP and phenolic hydroxyl groups of TA. TA–PVP complex acquires a negative charge because of deprotonation of the phenol groups. The formation of water soluble anionic TA–PVP complexes was observed at a pH of 7.5 and higher pH values [107]. Such TA–PVP complexes are very promising for the film deposition by advanced colloidal methods.

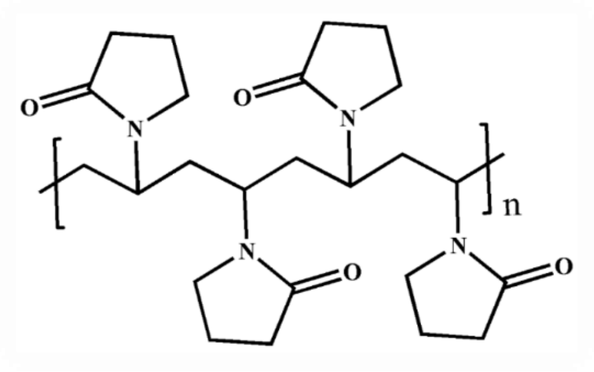

Figure 6-2 Chemical structure of PVP

The goal of this investigation was the application of the anionic TA–PVP complexes as a charging, dispersing agent for EPD to fabricate TA–PVP films and composites.

6.2 Complex formation and film formation

TA films cannot be deposited by EPD due to mutual electrostatic repulsion and poor film forming properties of relatively small size of TA molecules. Electrically neutral PVP cannot form deposit by EPD method, either. In contrast, the mixture of 1 g L^{-1} PVP and 1 g L^{-1} TA solutions allowed for the formation of anodic films. Fig 6-3 shows the relationship between deposit mass and deposition time for TA-PVP complexes. The increase of the deposit mass with deposition time indicated the formation of TA-PVP films. The film thickness can be varied in the range of 0–5 μm with increasing deposition time. EPD is a simple one-step method, which allows for film formation at relatively high deposition rates.

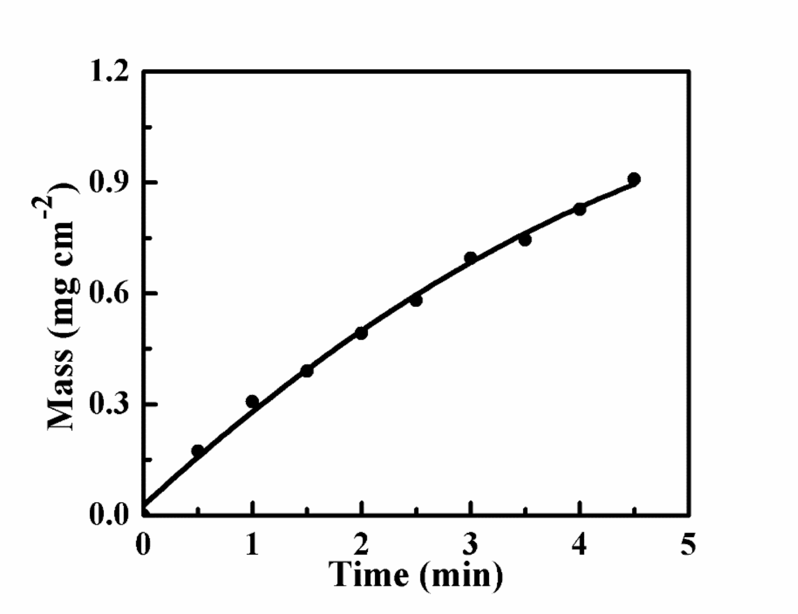

Figure 6-3 Deposit mass versus deposition time for solutions, containing 1 g L^{-1} TA and 1 g L^{-1} PVP in ethanol, at a deposition voltage of 30 V

For comparison, the fabrication of TA–PVP films by LbL assembly[107] is a complicate and time-consuming method, which needs more than 24 steps to deposit films with thickness less than 60 nm. The film formation mechanisms involved various processes and interactions, such as electrode reactions, depletion forces and other electrode processes, which promoted the coagulation of inorganic particles and polymers. Fig 6-4 shows an SEM image of the TA-PVP film prepared by EPD method. The EPD method allowed for the formation of continuous crack free TA-PVP films.

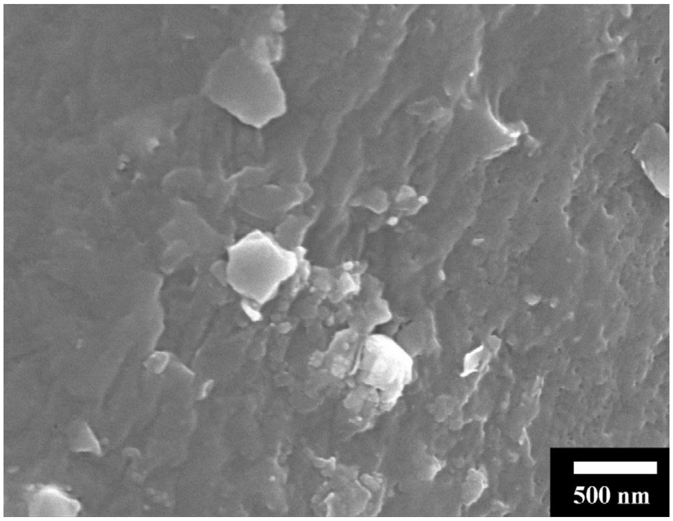

Figure 6-4 SEM image of a film prepared from a solution, containing 1 g L^{-1} TA and 1 g L^{-1} PVP in ethanol, at a deposition voltage of 30 V

The deposited material was studied by UV–vis and FTIR methods. Fig 6-5 shows the UV–vis and FTIR spectra of the deposited material. The UV–vis spectrum exhibits an absorption peak at ~210 nm and a broad absorption centered at ~300 nm. The study of the TA spectra in solutions[107] indicated that the acidic and neutral forms of TA exhibit two absorption peaks centered at ~223 nm and at ~283 nm. The spectra of TA at higher pH showed two peaks at longer wavelength, i.e., at ~245 and ~323 nm[107], which were assigned to ionized form of TA molecules[108] , resulting from ionization of the phenolic hydroxyl groups of galloyl groups of TA. The analysis of the TA films showed absorptions at 215 nm and broadened peak at 270 nm, related to the protonated form of TA. These results confirmed the incorporation of TA into the EPD films.

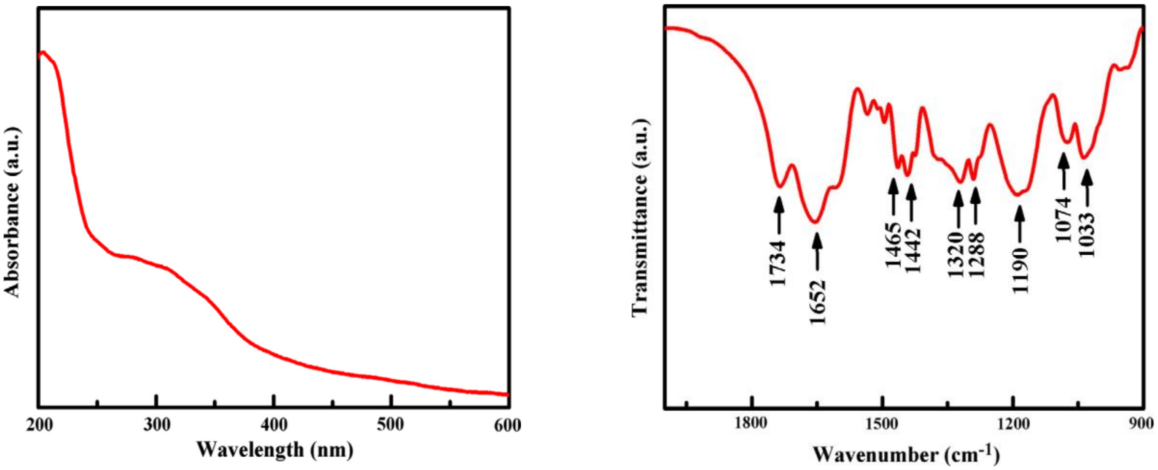

Figure 6-5 (a) FTIR spectrum and (b) UV–vis spectrum of a deposit, prepared from a solution, containing 1 g L^{-1} TA and 1 g L^{-1} PVP in ethanol at a deposition voltage of 30 V

The FTIR result exhibits a absorption peak at 1033 cm^{-1}, which was attributed to bending C–H vibrations[109] of TA and PVP. The aryl–oxygen stretching vibrations of the TA molecules resulted in a peak at 1074 cm^{-1} [52]. The bending vibrations of OH groups[109] of TA contributed to broad peak, centered at 1190 cm^{-1}. The C–O stretching vibrations[49, 52, 110] of TA resulted in peaks at 1288 and 1320 cm^{-1}. The absorptions at 1442 and 1465 cm^{-1} resulted from C–H stretching in PVP ring and in main chain, deformation and C–N stretching[111]. The broad adsorption at 1652 cm^{-1} resulted from C=O stretching vibration of PVP after complexation with TA and C–C stretching vibrations of the aromatic ring of TA. The absorption at 1734 cm^{-1} was assigned to C=O stretching vibration[112] of TA.

The FTIR and UV–vis data, coupled with deposition yield results and SEM observations indicated the deposition of TA–PVP films. The deposition mechanism was based on the formation of anionic TA–PVP complexes and their electrophoretic accumulation at the substrate[54]. In such TA–PVP complexes, the carbonyl groups of PVP and phenolic hydroxyl groups of TA are bonded together based on the hydrogen bonding mechanism. The schematic is shown in Fig 6-6.

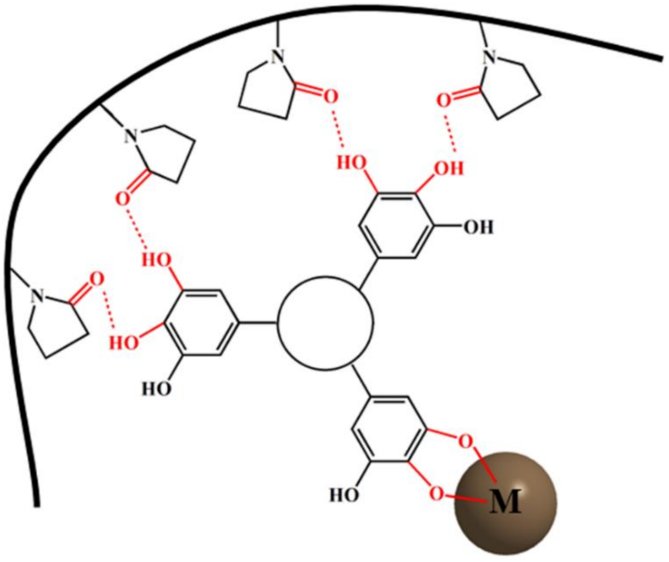

Figure 6-6 bonding and adsorption mechanism of TA-PVP complexes

The negatively charged complexes can be deposited by EPD. The local pH decrease at the anode[94], the charge neutralization of the TA–PVP and binding properties of the relatively large PVP macromolecules promoted deposit formation on the anode surface. The accumulation of TA–PVP complexes at the electrode surface and the protonation of the phenolic hydroxyl groups of TA resulted in the TA bonding to different PVP molecules. In this case the TA molecules, containing multiple galloyl groups, acted as cross-linkers and promoted the formation of insoluble TA–PVP films. The possibility of the deposition of TA–PVP films paved the way for the fabrication of various inorganic materials films using TA–PVP complexes as dispersing, charging and film forming agents.

6.3 Dispersion and deposition of inorganic materials using TA-PVP complexes

TA–PVP solutions for EPD contained 1 g L^{-1} TA, 1 g L^{-1} PVP and 1 mM NaOH in ethanol. Organic–inorganic composite coatings have been successfully achieved by using EPD method with huntite, hydrotalcite, MnO_2, TiO_2, Pd, TiN, MWCNT or their mixtures in the TA–PVP solutions.

Fig 6-7 shows the SEM images of the formation of uniform films, containing huntite nanoplatelets and hydrotalcite clay particles in the TA–PVP matrix. Fig 6-8 shows the SEM images of continuous and crack free films containing MnO_2 and TiO_2 nanoparticles.

The mechanism involved adsorption of TA–PVP complexes on different particle surfaces. The chemical structure of TA contains the galloyl groups, which can form chelates with different metal atoms. Previous investigation showed that some galloyl group family molecules such as gallic acid can be used as a charging and dispersing agent for the EPD of metal oxide particles[37]. The adsorption of gallic acid on inorganic particles was beneficial for its application as a dispersant.

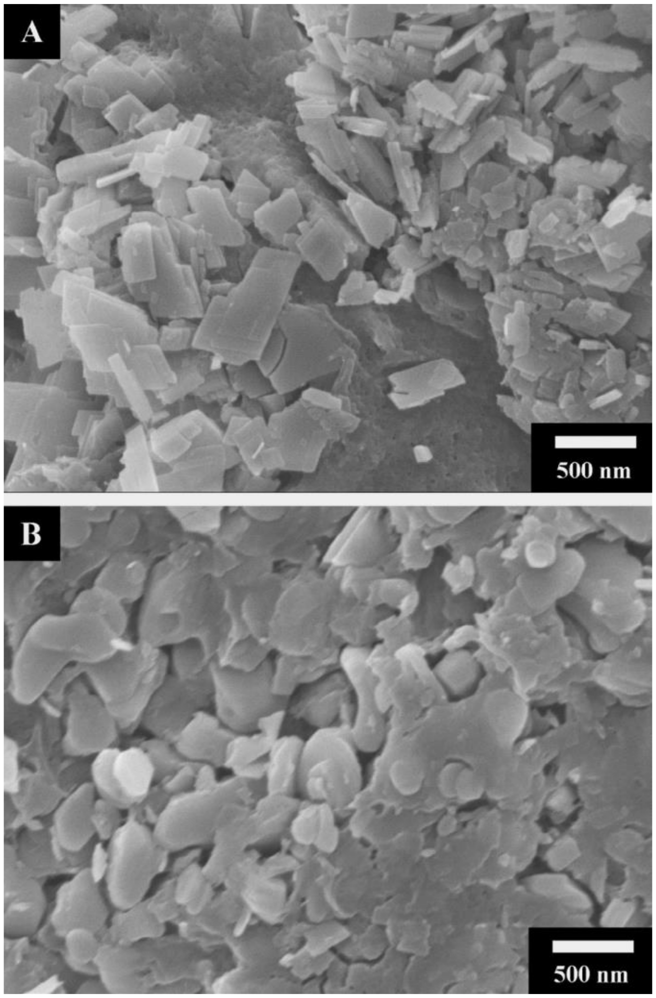

Figure 6-7 SEM images of films, prepared at a deposition voltage of 30 V from (A) 4 g L^{-1} huntite and (B) 4 g L^{-1} hydrotalcite suspensions in ethanol, containing 1 g L^{-1} TA and 1 g L^{-1} PVP

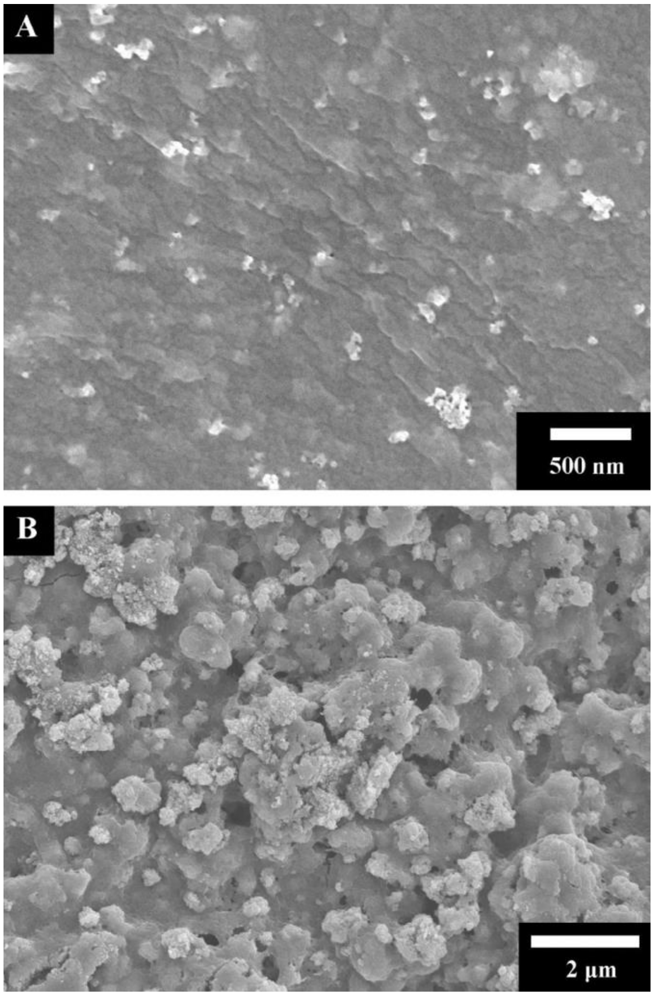

Figure 6-8 SEM images of films, prepared at a deposition voltage of 30 V from (A) 4 g L^{-1} MnO_2 and (B) 4 g L^{-1} TiO_2 suspensions in ethanol, containing 1 g L^{-1} TA and 1 g L^{-1} PVP

However, only limited number of materials was deposited by EPD using gallic acid due to the relatively weak adsorption of single galloyl group. The larger size and multiple adsorption sites of TA offer many advantages. The adsorption of TA on inorganic particles

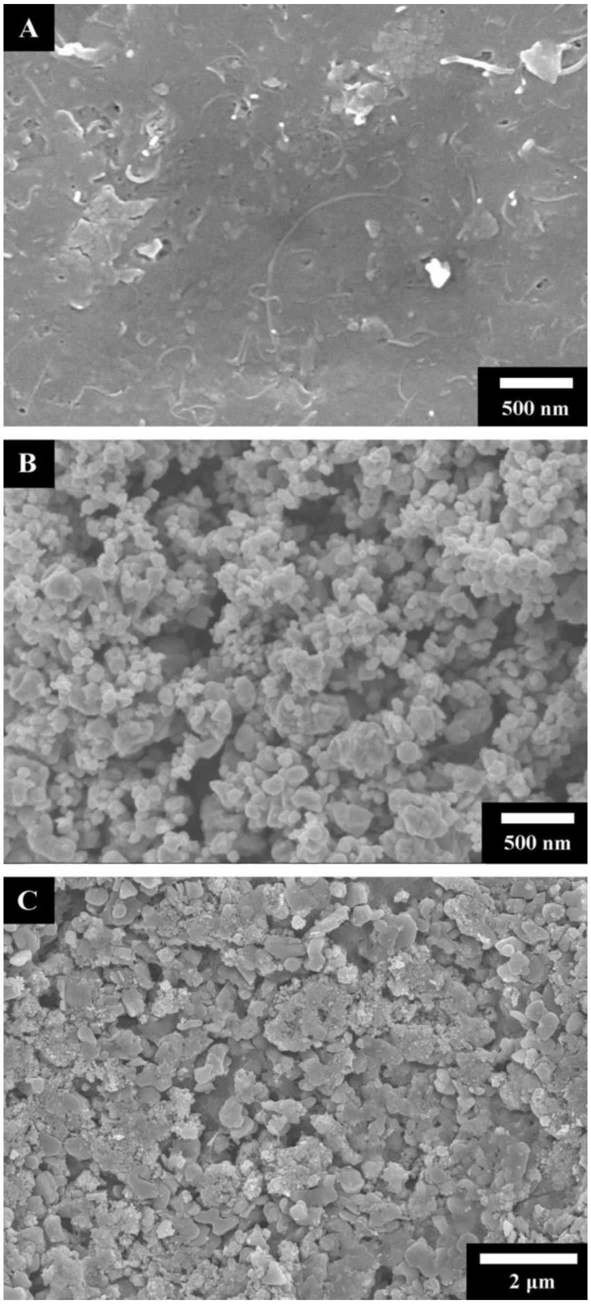

Figure 6-9 SEM images of films, prepared at a deposition voltage of 30 V from (A) 1 g L^{-1} CNT, (B) 4 g L^{-1} Pd and (C) 4 g L^{-1} TiN suspensions in ethanol, containing 1 g L^{-1} TA and 1 g L^{-1} PVP

involved complexation of metal atoms on particle surface with the galloyl groups, which is similar to gallic acid. The adsorbed TA can impart a charge to the inorganic particles and allows for their EPD. Moreover, the film forming and binding properties of the TA–PVP complexes offer additional benefits for film formation.

The TA–PVP complexes acts as a binder, improves deposit adhesion and prevents film cracking. In this strategy, the adsorption of binders on the particle surface is of critical importance. The adsorption properties of the PVP can be improved by the formation of PVP–TA complexes, containing chelating galloyl groups of TA. Thus, the TA–PVP complexes can disperse and deposit different particles.

Fig 6-9 shows an SEM image of the composite film, containing MWCNT, Pd metal and TiN particles in the TA–PVP matrix. Previous investigations showed that aromatic molecules interact strongly with sidewalls of carbon nanotubes through π –π stacking interaction [53]. Moreover, the adsorption mechanisms involved complexation of Pd and Ti atoms with TA on the particle surfaces. The porosity can result from packing of the particles and gas evolution at the electrode.

The films prepared by EPD have wide applications, utilizing functional properties of the deposited materials and PVP–TA complexes. Huntite and hydrotalcite can be used as advanced flame retardant additives for polymer coatings and polymer based composites[113, 114]. TiO_2, TiN, Pd, MnO_2 are important materials for catalytic, electronic, biomedical and energy storage applications[115, 116]. Besides, using TA–PVP as dispersant will not damage the structure of MWCNT or cause degradation of mechanical and electrical properties. The results presented above indicated that unique adsorption properties of TA can be used for the deposition of various materials. Therefore, the approach based on the use of TA–PVP complexes is promising for the co-deposition of different materials.

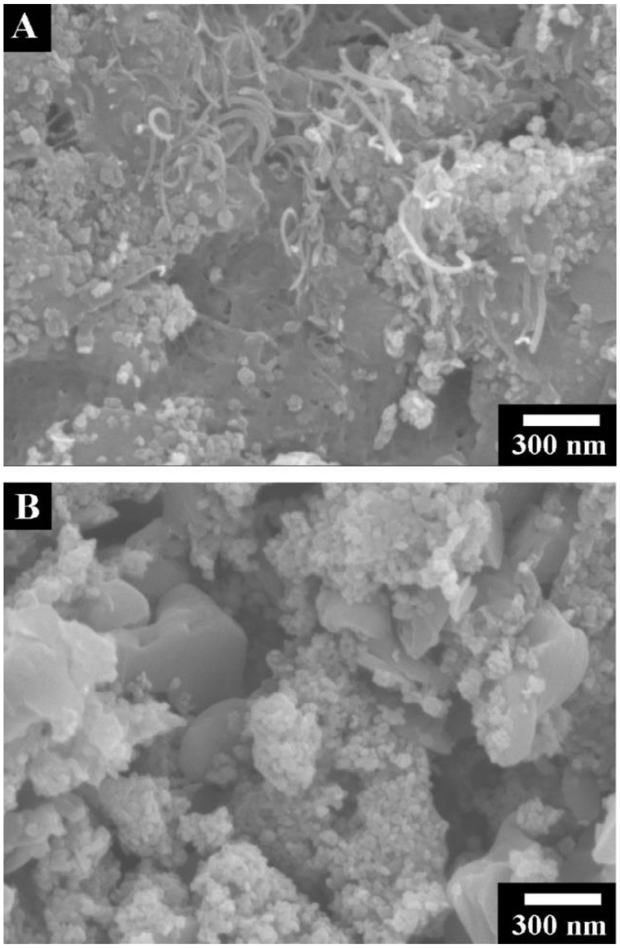

Figure 6-10 SEM images of composite films, prepared at a deposition voltage of 30 V from (A) 1 g L^{-1} CNT and (B) 4 g L^{-1} hydrotalcite suspensions in ethanol, containing 4 g L^{-1} TiO$_2$, 1 g L^{-1} TA and 1 g L^{-1} PVP

From our investigation, we prepared composite TiO_2 – MWCNT and TiO_2 – hydrotalcite films for catalysis application. The Fig 6-10 showed the SEM of deposited films contained particles of TiO_2 – MWCNT and TiO_2 – hydrotalcite composites.

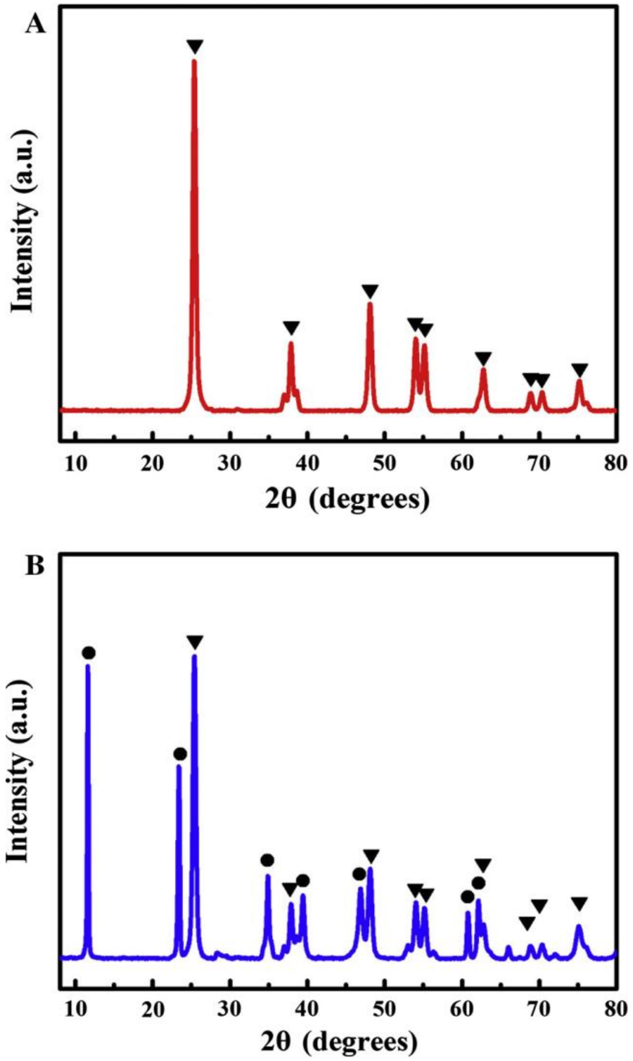

Figure 6-11 XRD of composite films, prepared at a deposition voltage of 30 V from (A) 1 g L^{-1} CNT and (B) 4 g L^{-1} hydrotalcite suspensions in ethanol, containing 4 g L^{-1} TiO_2, 1 g L^{-1} TA and 1 g L^{-1} PVP (● – TiO_2 anatase, ▼– hydrotalcite)

The Fig 6-11 presents XRD diffraction patterns, which showed peaks of the individual components, corresponding to JCPDS file 21-1272 for TiO_2 and JCPDS file 22-700 for hydrotalcite. The formation of composite films was confirmed by the XRD studies.

6.4 Conclusion

TA–PVP films can be obtained from the solutions of TA–PVP complexes. However, no EPD was achieved from the individual TA or PVP solutions. In the EPD method, the TA–PVP complexes were used as dispersing, charging and film forming agents for different materials and the fabrication of composites. The obtained films have widely applications based on the functional properties of TA and catalytic, flame retardant, charge storage and electronic properties of the co-deposited materials.

In this investigation, we developed a new method to fabricate TA–PVP films and composite material. The deposition mechanism is based on EPD of charged TA–PVP complexes. TA showed strong adsorption on various materials. The unique adsorption properties of TA provided a capability of dispersion, charging and EPD of organic and inorganic materials of different types using TA–PVP complexes. Moreover, the method allowed co-deposition of different materials and formation of composite films.

The analysis of the deposition mechanism indicated that similar approach can be used for the EPD of other electrically neutral polymers with hydrogen accepting carbonyl groups and phenolic molecules, which cannot be deposited individually.

7. Dispersion and heterocoagulation method for the fabrication of MnO_2-MWCNT composites for supercapacitors

7.1 Motivation and origin

Lauryl gallate (LG) is a promising dispersant[117-119] for colloidal processing of inorganic nanoparticles. The chemical structure of LG (Fig 7-1) allows for the interactions of this molecule with different materials. The galloyl group of LG promotes its adsorption on inorganic particles. Galloyl group of LG forms chelates[117] with metal atoms based on catecholate type of bonding[37]. Long hydrocarbon chain of LG promotes its adsorption on organic materials. The efficient stabilization mechanism of LG is based on steric effect of the hydrocarbon chain of adsorbed LG.

The strong adsorption of LG on inorganic and organic materials have prompted research efforts focused on the development of a heterocoagulation method. A promising development was the fabrication of MnO_2-MWCNT composites for application in electrochemical supercapacitors, which showed enhanced capacitive properties. The use of colloidal methods for the fabrication of MnO_2-MWCNT nanocomposites offers many advantages, such as prevention of MnO_2 agglomeration and MWCNT degradation. The goal of my investigation was the development of MnO_2-MWCNT composites electrode by using LG as a co-dispersant and heterocoagulating agent.

7.2 Adsorption and dispersion of LG on MnO_2 and MWCNT

Despite the impressive progress achieved in the technology of MnO_2-MWCNT electrodes, the major difficulties come from poor utilization of capacitive properties of MnO_2. The ability to achieve high capacitance at fast charge and discharge conditions is of critical importance for the development of high power supercapacitor. Difficulties are mainly attributed to the co-dispersion MnO_2 and MWCNT. One of the challenges in the development of MnO_2-MWCNT composite electrodes is the achievement of good dispersion and mixing of the individual components.

Using LG as a co-dispersant offered a good problem solution. The chelating bonding of LG to surface MnO_2 atoms allowed for LG adsorption on MnO_2 particles. Similar to other molecules, containing long hydrocarbon chains, the adsorption of LG on MWCNT involved hydrophobic interactions [120-122]. Therefore, the adsorption of LG on MnO_2 and MWCNT resulted in the dispersion of MnO_2 and MWCNT (Fig 7-2). However, mixing of such suspensions together resulted in the co-precipitation of MnO_2 and MWCNT and formation of black precipitation. It is suggested that co-precipitation of the materials resulted from links formation between MnO_2 particles and MWCNT by LG (Fig 7-1 B), which resulted in heterocoagulation and precipitation of both materials.

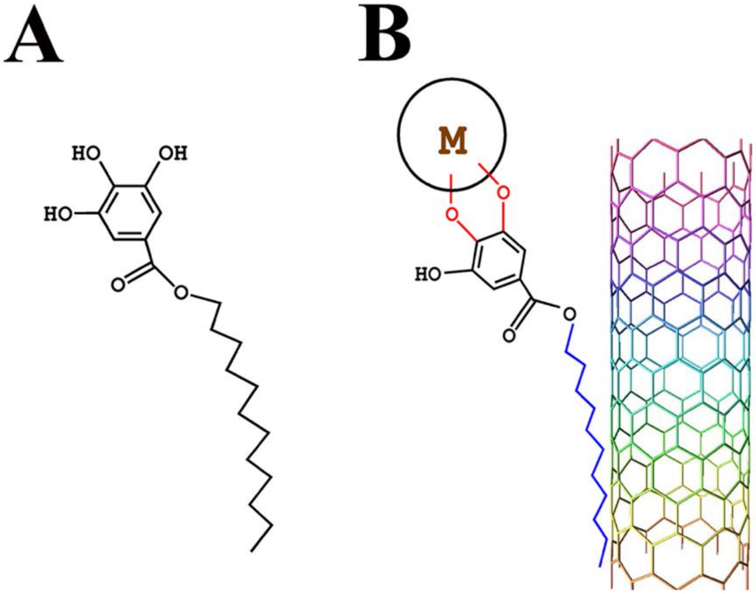

Figure 7-1 (A) Chemical structure of LG, (B) adsorption of LG on metal oxide and MWCNT

In this experiment, manganese dioxide nanoparticles were prepared by the reduction of aqueous $KMnO_4$ solutions with ethanol, as it was described in chapter 4.4. The concentration of MnO_2 and MWCNT for co-precipitation is 4 g L^{-1} and 1 g L^{-1}. Both materials were dispersed in 50% water – 50% ethanol solution, containing 1 g L^{-1} of LG as a dispersant. From our previously work, we found that MnO_2-MWCNT electrode can reach its maximum capacitance if the mass ratio of MnO_2 to MWCNT is 4 to 1[39]. After mixing both solutions with the same volume, the black precipitation forms immediately.

Figure 7-2 Sedimentation test in a mixed ethanol (50%) – water (50%) solvent, containing 1 g L^{-1} LG and (a) 4 g L^{-1} MnO_2 (b) 1 g L^{-1} MWCNT (c) 2 g L^{-1} MnO_2 and 0.5 g L^{-1} MWCNT

The TGA and DTA studies confirmed the formation of a composite material (Fig 7-3). TGA data showed mass loss, related to dehydration[123] of MnO_2 below ~200ºC, additional steps in the range of 200-250ºC and 300-500 ºC were attributed to burning out of adsorbed LG and MWCNT, the mass loss above 880 ºC resulted from MnO_2 to Mn_3O_4 transformation[124, 125]. The exothermic peaks in the DTA data corresponded to the steps in mass loss and resulted from burning out of LG, MWCNT and formation of Mn_3O_4. The heterocoagulation strategy is not limited to the use of MnO_2 nanoparticles. The sedimentation tests showed a similar behavior of TiO_2 nanoparticles and formation of

TiO_2-MWCNT composites. The adsorption of LG on MnO_2, TiO_2 and MWCNT was confirmed by FTIR data (Fig 7-4).

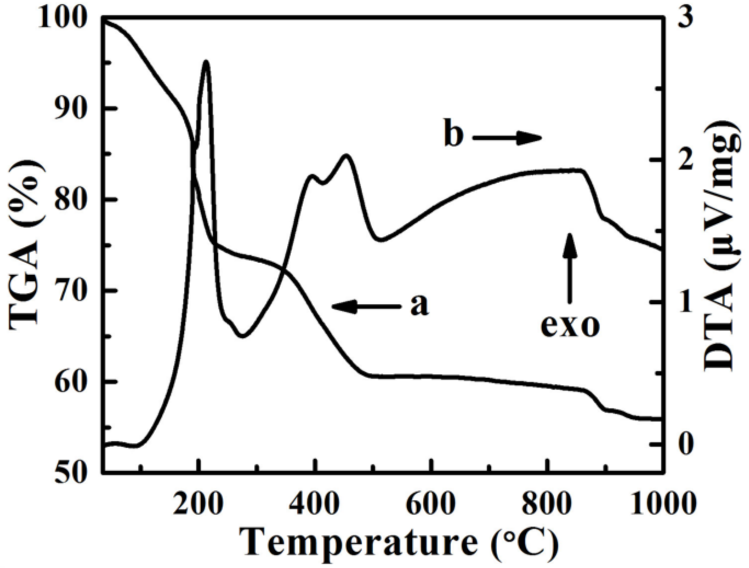

Figure 7-3 (a) TGA and (b) DTA data for material, prepared by co-precipitation from solution, containing 1 g L^{-1} MWCNT, 1 g L^{-1} LG and 4 g L^{-1} MnO_2 in a water-ethanol solvent

The FTIR result exhibited an absorption peak at 1635 cm^{-1} [126], which was attributed to bending C–C stretching vibrations of the aromatic ring of MWCNT. The bending vibrations of OH groups of LG contributed to broad peak, centered at 1125 cm^{-1}. The adsorption at 1404 cm^{-1} and 1275 cm^{-1} [127]was attributed to C=O vibrations of carboxylate of LG. The broad adsorption at 623 cm^{-1} and 511 cm^{-1} [128] resulted from Mn–O stretching vibration of MnO_2. The absorption at 942 cm^{-1} and 453 cm^{-1} [129] was assigned to Ti–O stretching vibration of TiO_2. These results prove the formation of MnO_2-MWCNT and TiO_2-MWCNT and co-dispersion by LG.

The TGA-DTA and FTIR data has proved the formation of MnO_2-MWCNT composite, containing LG. The co-precipitation of MnO_2 and MWCNT was beneficial for mixing of the individual components. The ratio of MnO_2 and MWCNT composite can be easily varied by changing the concentration of MnO_2 and MWCNT.

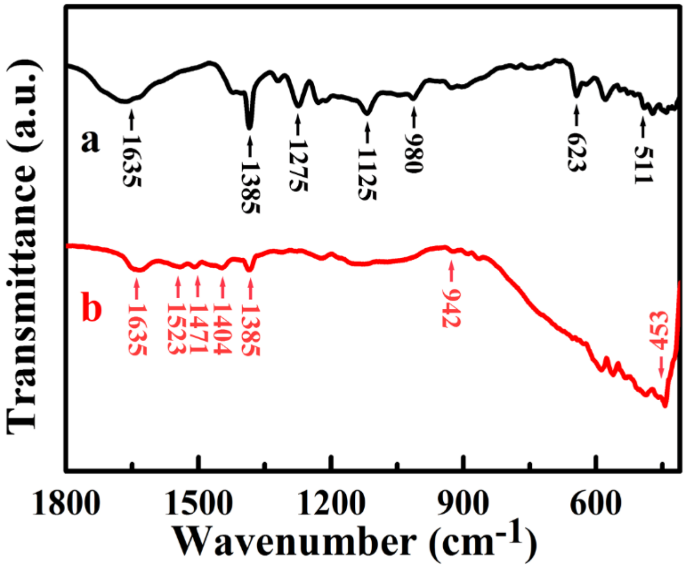

Figure 7-4 FTIR spectra of materials prepared by co-precipitation from solutions, containing 1 g L^{-1} MWCNT, 1 g L^{-1} LG and (a) 4 g L^{-1} MnO_2 or (b) 4 g L^{-1} TiO_2 in a water-ethanol solvent

7.3 Electrochemical characterization of composite electrodes

The MnO_2-MWCNT composite was mixed with PVB (5% total mass of active material) as a binder and formed a slurry to impregnate into current collectors. In this investigation we targeted the fabrication of electrodes with relatively high active mass loadings, which was 30 mg cm^{-2}. Result studies[130] shows the mass loading of efficient electrodes must be above 10 mg cm^{-2} for practical applications.

Nickel foams are widely used for current collector of supercapacitor electrodes. The porous structure has high surface area, good mechanical properties and light weight. But the conductivity of nickel foam still need to be increased to fabricate high power density supercapacitor. From my investigation, graphene coated nickel foam has porous structure and excellent conductivity, which can act as an excellent current collector and increase the capacitance behavior.

We obtained Ni foam and Ni foam coated by ~5 layers of graphene. The SEM images of Ni foam (Fig 7-5 (A,B)) and graphene coated Ni foam (Fig 7-5 (C,D)) current collectors showed non-damaged framework with large pore size of 100-200 μm. Such porosity is ideally suited for the impregnation with active material and fabrication of electrodes with high active mass loading.

The comparison of images at low magnification (Fig 7-5 (A,C)) and high magnification (Fig 7-5 (B,D)) indicated that Ni foam was uniformly coated with graphene. The high magnification images showed that the surface of coated foam is relatively rough, compared to surface of uncoated Ni foam. The electrochemical testing of the graphene coated Ni foam, showed that foam capacitance was less than 1.55 mF cm^{-2} in the scan rate range of 2-100 mV s^{-1}.

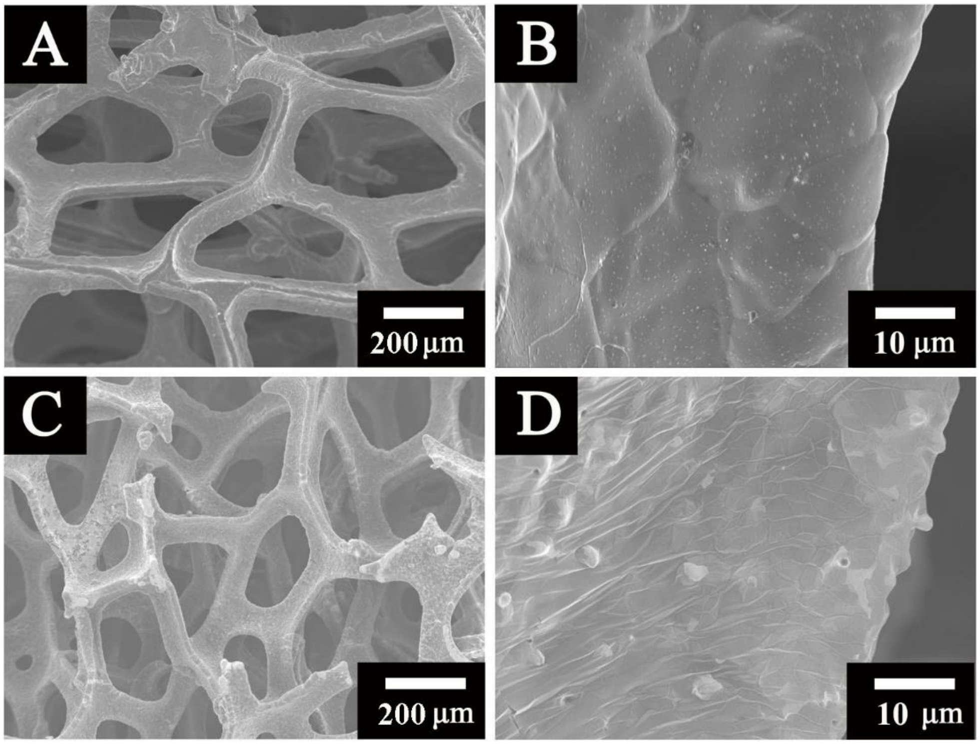

Figure 7-5 SEM images of Ni foam (A, B) and Graphene coated Ni foam (C, D) current collectors at different magnifications

Testing results of impregnated foams presented below indicated that the capacitance of the graphene coatings was negligibly small, compared to the capacitance of the impregnated active material. The electrodes, prepared without LG and using Ni foam showed poor capacitive behavior, as indicated by the low areas of CVs and low capacitance, which decreased rapidly with increasing scan rate (Fig 7-6 A, D(a)). The electrodes, prepared by the heterocoagulation method using Ni foam showed the increase in the CV areas (Fig 7-6 b) and higher capacitances (Fig 7-6 D(b)) at scan rates in the range of 2-100 mV s^{-1}. Further improvement in the capacitive behavior, was achieved using the heterocoagulation method and graphene coated Ni foam (Fig 7-6 C, D(c)). The increase in capacitance is especially evident at scan rates of 50 and 100 mV s^{-1}.

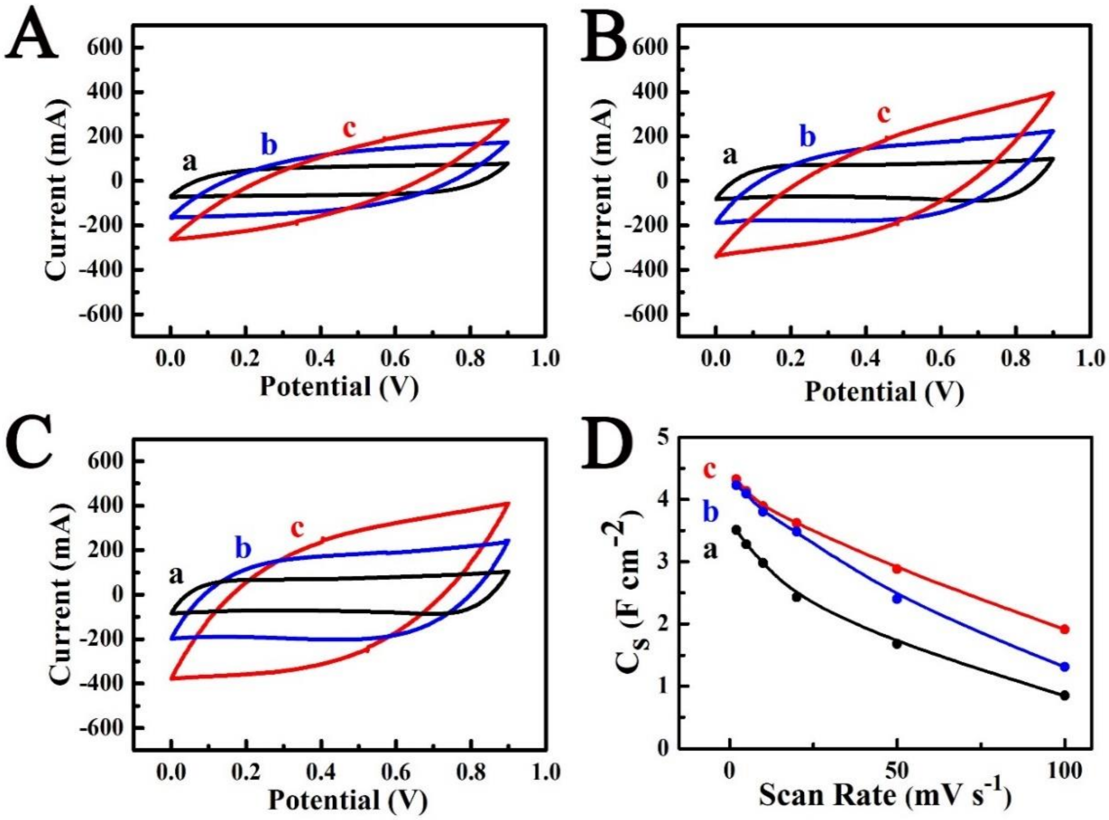

Figure 7-6 Cyclical voltammetry and specific capacitance results of (A, D (a)) MnO$_2$-MWCNT impregnated into nickel foam, (B, D (b)) MnO$_2$-MWCNT with LG impregnated into Ni foam and (C, D (c)) MnO$_2$-MWCNT with LG impregnated into graphene coated Ni foam with the scan rate of (a) 20mV s^{-1}, (b) 50mV s^{-1} and (c) 100mV s^{-1}

The impedance data (Fig 7-7 A) presented in the Nyquist plot shows reduced resistance R=Z' of the electrodes, prepared using the heterocoagulation method. The frequency dependencies of capacitance (Fig 7-7 B,C), calculated from the impedance data showed typical relaxation type dispersions[131], involving decrease in the real part of capacitance C' with increase in frequency and maximum in the imaginary part C" at the relaxation frequency. The electrodes, prepared by the heterocoagulation method using graphene coated current collectors showed the highest capacitance at scan rates of 2-100 mV s^{-1} and significantly higher capacitances compared to electrodes prepared without LG (Fig 7-6 A, D(a)). The capacitance decreased from 4.4 F cm^{-2} (under 2 mV s^{-1}) to 2.3 F cm^{-2} (under 100 mV s^{-1}), showing good capacitance retention of 53 %. Good capacitance retention at a high scan rate is important for the development of high power supercapacitor. The electrodes, prepared using graphene coated Ni foams showed lower impedance, higher C' and higher relaxation frequency, corresponding to C" maximum, compared to Ni foam based electrodes (Fig 7-7). The higher relaxation frequency indicates improved capacitance retention at higher frequencies.

From the testing results, we observed significant improvement in performance of electrodes prepared using graphene coated Ni foam. Testing of graphene coated Ni foam without active material showed that the capacitance of such current collectors is negligibly low, compared to the capacitances of the active materials. Therefore, the contribution of current collectors to the total capacitance cannot explain the difference in capacitances of electrodes, prepared using uncoated and coated Ni foams. It is suggested that graphene coating can reduce contact resistance, preventing the formation of an oxide layer on the Ni surface. Also, it has high conductivity and low resistance. The relatively rough surface of the coated foam is also beneficial for the reduction of the contact resistance. As a result, the graphene coating can facilitate charge transfer and increase capacitance of the electrodes. This effect is especially evident at high charge-discharge rates.

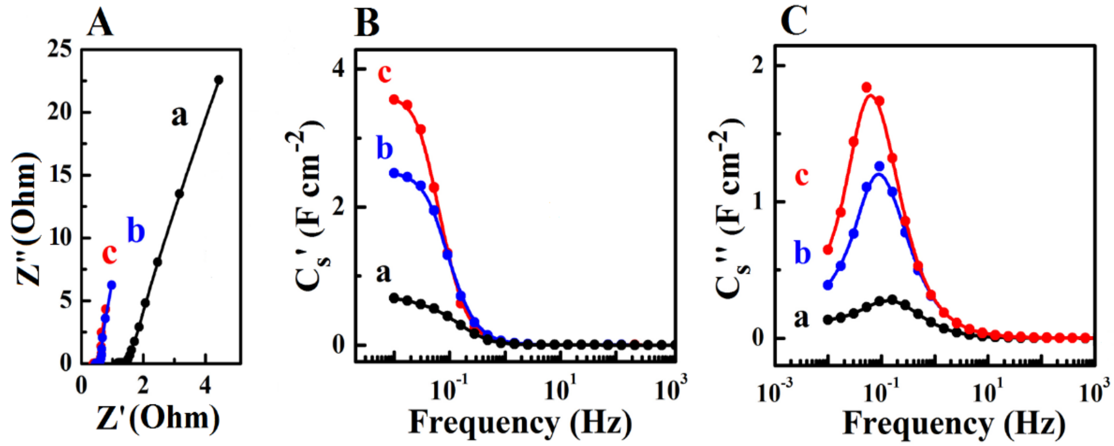

Figure 7-7 (A)Nyquist plot of complex impedance and frequency dependencies of (B) real C' and (C) imaginary C'' components of complex capacitance for MnO_2 – MWCNT composites: (a) mixed without dispersant and impregnated into Ni foam, (b) mixed using LG and impregnated into Ni foam, (c) mixed using LG and impregnated into graphene coated Ni foam.

7.4 Conclusions

In this work, we demonstrate a heterocoagulation method based on the use of LG as a co-dispersant for MnO_2 and MWCNT. The results obtained by the heterocoagulation method indicated that LG provides good adsorption and dispersion of individual components and forms strong linkage between MnO_2 and MWCNT, facilitating their mixing. Thus the problems related to MnO_2 particles agglomeration and MWCNT degradation can be avoided. This method provides a simple and versatile way to fabricate electrode for supercapacitor. Testing results provide an insight into the mechanism of co-dispersion of MnO_2 and MWCNT, which resulted in improved mixing and good electrochemical performance. The electrochemical testing results presented above indicated that dispersion and mixing of MnO_2 and MWCNT are critical for the development of efficient electrodes. Also, using graphene coated nickel foam as a current collector allow significantly increase of the capacitance and retention at high scan rate. As a result, improved capacitive behavior was observed.

The approach developed in this investigation allowed for high capacitance and excellent capacitance retention at high charge-discharge rates, which provides a possibility to fabricate high power density supercapacitor.

8. Conclusions

In this work, we investigated the fabrication of organic-inorganic composite materials by new colloidal methods. New EPD strategies and bath formulations have been developed to fabricate multi-functional composite films.

We found that PAZO can be used as universal dispersant for various materials. PAZO exhibited unique adsorption on different materials due to the unique structure of this polymer. The aromatic anionic PAZO monomers, containing chelating salicylate ligands provided multiple adsorption sites for PAZO and allowed for efficient electrosteric dispersion and EPD. Using PAZO as a co-dispersant and film forming agent allowed for EPD of composites, containing metals, metal oxides, nitrides, polymers, minerals etc. The results of this investigation paved the way for EPD of other composites utilizing properties of different functional materials and unique physical properties of PAZO.

TA provided multiple adsorption sites to form chelation with metal oxides due to multiple phenolic groups of TA. Besides, the phenolic group could attach with other polymers, like PVP, containing carbonyl group and forms complexes with TA through hydrogen bonding. The multiple adsorption sites of TA-PVP complexes imparted good adsorption properties to TA-PVP complexes. The unique adsorption properties of TA, coupled with the binding properties of PVP, provided a capability of dispersion, charging and EPD of organic and inorganic materials of different types using TA–PVP complexes. This results showed new strategies for the fabrication of various organic-inorganic composites.

Some dispersing agent could not only provide strong adsorption and dispersion of inorganic and organic particles, but also formed strong linkage between them. We found the unique chemical structure of LG provides the possibility of LG to adsorb on MnO_2 and MWCNT. The uniform composites could be obtained through the linkage formation and the ratio of individual component could be varied. The MnO_2-MWCNT electrode, containing LG, showed a higher capacitance and better retention comparing to MnO_2-MWCNT without LG.

This investigation presented a promising, low-cost and simple colloidal method. These dispersing agents have excellent adsorption and dispersion on various organic and inorganic materials. The results pave the way for the fabrication of multi-functional materials for various applications.

9. Reference

1. Ferrari, B. and R. Moreno, *EPD kinetics: a review*. Journal of the European Ceramic Society, 2010. **30**(5): p. 1069-1078.
2. Cao, G., *Synthesis, Properties and Applications*. 2004: World Scientific.
3. Derjaguin, B. and L. Landau, *Theory of the stability of strongly charged lyophobic sols and of the adhesion of strongly charged particles in solutions of electrolytes.* Acta physicochim. URSS, 1941. **14**(6): p. 633-662.
4. Zhitomirsky, I., *Cathodic electrodeposition of ceramic and organoceramic materials. Fundamental aspects.* Advances in colloid and interface science, 2002. **97**(1): p. 279-317.
5. Hotze, E.M., T. Phenrat, and G.V. Lowry, *Nanoparticle aggregation: challenges to understanding transport and reactivity in the environment.* Journal of environmental quality, 2010. **39**(6): p. 1909-1924.
6. Verwey, E. and J.T.G. Overbeek, *Theory of the stability of lyophobic colloids.* Journal of Colloid Science, 1955. **10**(2): p. 224-225.
7. Sader, J.E. and D.Y. Chan, *Electrical double-layer interaction between charged particles near surfaces and in confined geometries.* Journal of colloid and interface science, 1999. **218**(2): p. 423-432.
8. Sun, F., X. Pang, and I. Zhitomirsky, *Electrophoretic deposition of composite hydroxyapatite–chitosan–heparin coatings.* Journal of materials processing technology, 2009. **209**(3): p. 1597-1606.

9. Van der Biest, O.O. and L.J. Vandeperre, *Electrophoretic deposition of materials.* Annual Review of Materials Science, 1999. **29**(1): p. 327-352.

10. Farrokhpay, S., *A review of polymeric dispersant stabilisation of titania pigment.* Advances in Colloid and Interface Science, 2009. **151**(1): p. 24-32.

11. Labib, M.E. and R. Williams, *The use of zeta-potential measurements in organic solvents to determine the donor—acceptor properties of solid surfaces.* Journal of colloid and interface science, 1984. **97**(2): p. 356-366.

12. Yamashita, K., M. Nagai, and T. Umegaki, *Fabrication of green films of single- and multi-component ceramic composites by electrophoretic deposition technique.* Journal of materials science, 1997. **32**(24): p. 6661-6664.

13. Van Tassel, J. and C. Randall, *Electrophoretic deposition and sintering of thin/thick PZT films.* Journal of the European Ceramic Society, 1999. **19**(6): p. 955-958.

14. Harbach, F. and H. Nienburg, *Homogeneous functional ceramic components through electrophoretic deposition from stable colloidal suspensions—I. Basic concepts and application to zirconia.* Journal of the European Ceramic Society, 1998. **18**(6): p. 675-683.

15. Okamura, S., T. Tsukamoto, and N. Koura, *Fabrication of ferroelectric BaTiO3 films by electrophoretic deposition.* Japanese journal of applied physics, 1993. **32**(9S): p. 4182.

16. Grosso, P., R. Rutherford, and D. Sargent, *Electrophoretic deposition of luminescent materials.* Journal of The Electrochemical Society, 1970. **117**(11): p. 1456-1459.

17. Sarkar, P. and P.S. Nicholson, *Electrophoretic deposition (EPD): mechanisms, kinetics, and application to ceramics.* Journal of the American Ceramic Society, 1996. **79**(8): p. 1987-2002.

18. Schwarzacher, W., *Electrodeposition: a technology for the future.* Interface, 2006. **15**(1): p. 32-35.

19. Zhitomirsky, I., *Electrophoretic deposition of organic–inorganic nanocomposites.* Journal of materials science, 2006. **41**(24): p. 8186-8195.

20. Sarkar, P., X. Huang, and P.S. Nicholson, *Zirconia/alumina functionally gradiented composites by electrophoretic deposition techniques.* Journal of the American Ceramic Society, 1993. **76**(4): p. 1055-1056.

21. Hamaker, H., *Formation of a deposit by electrophoresis.* Transactions of the Faraday Society, 1940. **35**: p. 279-287.

22. Hermans, J., *Sedimentation and electrophoresis of porous spheres.* Journal of Polymer Science, 1955. **18**(90): p. 527-534.

23. Ohshima, H., *On the general expression for the electrophoretic mobility of a soft particle.* Journal of colloid and interface science, 2000. **228**(1): p. 190-193.

24. Biesheuvel, P.M. and H. Verweij, *Theory of cast formation in electrophoretic deposition.* Journal of the American Ceramic Society, 1999. **82**(6): p. 1451-1455.

25. Ohshima, H., *Electrophoretic mobility of soft particles.* Colloids and Surfaces A: Physicochemical and Engineering Aspects, 1995. **103**(3): p. 249-255.

26. Lee, H., et al., *Mussel-inspired surface chemistry for multifunctional coatings.* science, 2007. **318**(5849): p. 426-430.

27. Young, G.A. and D. Crisp, *Marine animals and adhesion.* Adhesion, 1982. **6**: p. 19-39.

28. Lee, B.P., et al., *Mussel-inspired adhesives and coatings.* Annual review of materials research, 2011. **41**: p. 99.

29. Lee, H., B.P. Lee, and P.B. Messersmith, *A reversible wet/dry adhesive inspired by mussels and geckos.* Nature, 2007. **448**(7151): p. 338-341.

30. Petrone, L., *Molecular surface chemistry in marine bioadhesion.* Advances in colloid and interface science, 2013. **195**: p. 1-18.

31. Bahri, S., et al., *Adsorption and surface complexation study of L-DOPA on rutile (α-TiO2) in NaCl solutions.* Environmental science & technology, 2011. **45**(9): p. 3959-3966.

32. Cornard, J. and C. Lapouge, *Theoretical and spectroscopic investigations of a complex of Al (III) with caffeic acid.* The Journal of Physical Chemistry A, 2004. **108**(20): p. 4470-4478.

33. Jankovic, I.A., et al., *Surface modification of colloidal TiO2 nanoparticles with bidentate benzene derivatives.* The Journal of Physical Chemistry C, 2009. **113**(29): p. 12645-12652.

34. Yu, M. and T.J. Deming, *Synthetic polypeptide mimics of marine adhesives.* Macromolecules, 1998. **31**(15): p. 4739-4745.

35. Ye, Q., F. Zhou, and W. Liu, *Bioinspired catecholic chemistry for surface modification.* Chemical Society Reviews, 2011. **40**(7): p. 4244-4258.

36. Dalsin, J.L., et al., *Mussel adhesive protein mimetic polymers for the preparation of nonfouling surfaces.* Journal of the American Chemical Society, 2003. **125**(14): p. 4253-4258.

37. Ata, M., Y. Liu, and I. Zhitomirsky, *A review of new methods of surface chemical modification, dispersion and electrophoretic deposition of metal oxide particles.* RSC Advances, 2014. **4**(43): p. 22716-22732.

38. Wu, K., et al., *Electrophoretic deposition of poly [3-(3-N, N-diethylaminopropoxy) thiophene] and composite films.* Materials Chemistry and Physics, 2011. **125**(1): p. 210-218.

39. Wang, Y. and I. Zhitomirsky, *Electrophoretic deposition of manganese dioxide−multiwalled carbon nanotube composites for electrochemical supercapacitors.* Langmuir, 2009. **25**(17): p. 9684-9689.

40. Wu, K. and I. Zhitomirsky, *Electrophoretic deposition of ceramic nanoparticles.* International Journal of Applied Ceramic Technology, 2011. **8**(4): p. 920-927.

41. de Souza, F.S. and A. Spinelli, *Caffeic acid as a green corrosion inhibitor for mild steel.* Corrosion science, 2009. **51**(3): p. 642-649.

42. Barreto, W.J., et al., *Adsorption of caffeic acid on titanium dioxide: A spectroscopic study.* Spectrochimica Acta Part A: Molecular and Biomolecular Spectroscopy, 2012. **92**: p. 16-20.

43. Sun, Y. and I. Zhitomirsky, *Electrophoretic deposition of titanium dioxide using organic acids as charging additives.* Materials Letters, 2012. **73**: p. 190-193.

44. Pogorelyi, V., et al., *Adsorption of cinnamic and caffeic acids on the surface of highly dispersed silica from different solvents.* Colloid Journal, 2007. **69**(2): p. 203-211.

45. Dovbii, O., O. Kazakova, and N. Lipkovskaya, *The effect of the structure of cinnamic acid derivatives on their interaction with highly dispersed silica in aqueous medium.* Colloid Journal, 2006. **68**(6): p. 707-712.

46. Wang, Y. and I. Zhitomirsky, *Bio-inspired catechol chemistry for electrophoretic nanotechnology of oxide films.* Journal of colloid and interface science, 2012. **380**(1): p. 8-15.

47. Tunesi, S. and M.A. Anderson, *Surface effects in photochemistry: an in situ cylindrical internal reflection-Fourier transform infrared investigation of the effect of ring substituents on chemisorption onto titania ceramic membranes.* Langmuir, 1992. **8**(2): p. 487-495.

48. Ata, M. and I. Zhitomirsky, *Preparation of MnO2 and composites for ultracapacitors.* Materials and Manufacturing Processes, 2013. **28**(9): p. 1014-1018.

49. Dobson, K.D. and A.J. McQuillan, *In situ infrared spectroscopic analysis of the adsorption of aromatic carboxylic acids to TiO 2, ZrO 2, Al 2 O 3, and Ta 2 O 5 from aqueous solutions.* Spectrochimica Acta Part A: Molecular and Biomolecular Spectroscopy, 2000. **56**(3): p. 557-565.

50. Wu, K., Y. Wang, and I. Zhitomirsky, *Electrophoretic deposition of TiO 2 and composite TiO 2–MnO 2 films using benzoic acid and phenolic molecules as*

charging additives. Journal of colloid and interface science, 2010. **352**(2): p. 371-378.

51. Araujo, P.Z., P.J. Morando, and M.A. Blesa, *Interaction of catechol and gallic acid with titanium dioxide in aqueous suspensions. 1. Equilibrium studies.* Langmuir, 2005. **21**(8): p. 3470-3474.

52. Ata, M. and I. Zhitomirsky, *Electrophoretic nanotechnology of ceramic films.* Advances in Applied Ceramics, 2012. **111**(5-6): p. 345-350.

53. Wang, Y. and I. Zhitomirsky, *Effect of phenolic molecules on electrophoretic deposition of manganese dioxide–carbon nanotube nanocomposites.* Colloids and Surfaces A: Physicochemical and Engineering Aspects, 2010. **369**(1): p. 211-217.

54. Luo, D., T. Zhang, and I. Zhitomirsky, *Electrophoretic deposition of tannic acid–polypyrrolidone films and composites.* Journal of colloid and interface science, 2016. **469**: p. 177-183.

55. Wang, W., et al., *One-step synthesis of biocompatible gold nanoparticles using gallic acid in the presence of poly-(N-vinyl-2-pyrrolidone).* Colloids and Surfaces A: Physicochemical and Engineering Aspects, 2007. **301**(1): p. 73-79.

56. Kallay, N., et al., *Adsorption of organic acids on metal oxides: Application of the surface potential measurements.* Colloids and Surfaces A: Physicochemical and Engineering Aspects, 2007. **306**(1): p. 40-48.

57. Binner, J., *Advanced ceramic processing and technology*. Vol. 1. 1990: Noyes Data Corporation/Noyes Publications.

58. Zhitomirsky, I., *JOM-e Miner Met Mater Soc J 52; 2000.*

59. Brown, D. and F. Salt, *The mechanism of electrophoretic deposition.* Journal of Applied Chemistry, 1965. **15**(1): p. 40-48.
60. Hamaker, H. and E. Verwey, *Part II.—(C) Colloid stability. The role of the forces between the particles in electrodeposition and other phenomena.* Transactions of the Faraday Society, 1940. **35**: p. 180-185.
61. Verwey, E. and J.T.G. Overbeek, *1948Theory of the stability of lyophobic colloids*. Amsterdam: Elsevier.
62. Shane, M.J., et al., *Electrophoretic deposition of phosphors: II. Deposition experiments and analysis.* Journal of colloid and interface science, 1994. **165**(2): p. 334-340.
63. Shimbo, M., et al., *Electrophoretic deposition of glass powder for passivation of high voltage transistors.* Journal of the Electrochemical Society, 1985. **132**(2): p. 393-398.
64. Sasaki, T., et al., *Layer-by-layer assembly of titania nanosheet/polycation composite films.* Chemistry of materials, 2001. **13**(12): p. 4661-4667.
65. Griffiths, P., et al., *Charge on poly (ethylene imine): comparing electrophoretic NMR measurements and pH titrations.* Macromolecules, 2005. **38**(8): p. 3539-3542.
66. Rivas, B.L. and K.E. Geckeler, *Synthesis and metal complexation of poly (ethyleneimine) and derivatives,* in *Polymer Synthesis Oxidation Processes*. 1992, Springer. p. 171-188.

67. Cassagneau, T., F. Guérin, and J.H. Fendler, *Preparation and characterization of ultrathin films layer-by-layer self-assembled from graphite oxide nanoplatelets and polymers*. Langmuir, 2000. **16**(18): p. 7318-7324.

68. Bon, P., I. Zhitomirsky, and J. Embury, *Electrodeposition of composite iron oxide–polyelectrolyte films.* Materials chemistry and physics, 2004. **86**(1): p. 44-50.

69. Nagarajan, N., H. Humadi, and I. Zhitomirsky, *Cathodic electrodeposition of MnO x films for electrochemical supercapacitors.* Electrochimica Acta, 2006. **51**(15): p. 3039-3045.

70. Wu, L.-Q., et al., *Spatially selective deposition of a reactive polysaccharide layer onto a patterned template.* Langmuir, 2003. **19**(3): p. 519-524.

71. Wu, L.-Q., et al., *Voltage-dependent assembly of the polysaccharide chitosan onto an electrode surface.* Langmuir, 2002. **18**(22): p. 8620-8625.

72. Wu, L.-Q., et al., *Chitosan-mediated and spatially selective electrodeposition of nanoscale particles.* Langmuir, 2005. **21**(8): p. 3641-3646.

73. Pang, X. and I. Zhitomirsky, *Electrodeposition of nanocomposite organic–inorganic coatings for biomedical applications.* International Journal of Nanoscience, 2005. **4**(03): p. 409-418.

74. Mizuguchi, J., K. Sumi, and T. Muchi, *A highly stable nonaqueous suspension for the electrophoretic deposition of powdered substances.* Journal of the Electrochemical Society, 1983. **130**(9): p. 1819-1825.

75. Zhitomirsky, I., *Electrophoretic deposition of chemically bonded ceramics in the system CaO-SiO2-P2O5.* Journal of materials science letters, 1998. **17**(24): p. 2101-2104.

76. Liu, Y., K. Shi, and I. Zhitomirsky, *New colloidal route for electrostatic assembly of oxide nanoparticle–carbon nanotube composites.* Colloids and Surfaces A: Physicochemical and Engineering Aspects, 2014. **446**: p. 15-22.

77. Devaraj, S. and N. Munichandraiah, *High Capacitance of Electrodeposited* MnO_2 *by the Effect of a Surface-Active Agent.* Electrochemical and Solid-State Letters, 2005. **8**(7): p. A373-A377.

78. Brousse, T., et al., *Long-term cycling behavior of asymmetric activated carbon/*MnO_2 *aqueous electrochemical supercapacitor.* Journal of Power Sources, 2007. **173**(1): p. 633-641.

79. Brousse, T., M. Toupin, and D. Bélanger, *A Hybrid Activated Carbon-Manganese Dioxide Capacitor using a Mild Aqueous Electrolyte.* Journal of The Electrochemical Society, 2004. **151**(4): p. A614-A622.

80. Wang, Y., Y. Liu, and I. Zhitomirsky, *Surface modification of* MnO_2 *and carbon nanotubes using organic dyes for nanotechnology of electrochemical supercapacitors.* Journal of Materials Chemistry A, 2013. **1**(40): p. 12519-12526.

81. Jiang, R., et al., *Factors influencing* MnO_2*/multi-walled carbon nanotubes composite's electrochemical performance as supercapacitor electrode.* Electrochimica Acta, 2009. **54**(27): p. 7173-7179.

82. Taberna, P., P. Simon, and J.-F. Fauvarque, *Electrochemical characteristics and impedance spectroscopy studies of carbon-carbon supercapacitors.* Journal of the Electrochemical Society, 2003. **150**(3): p. A292-A300.

83. Goldenberg, L.M., et al., *Influence of the cation type on the DFB lasing performance of dye-doped azobenzene-containing polyelectrolytes.* Journal of Materials Chemistry C, 2014. **2**(40): p. 8546-8553.

84. Maaland, S.A., et al., *Adsorption of fibrinogen on polyionic azobenzene layer-by-layer film using photoisomerization.* Polymer Preprints, 2008. **49**(1): p. 990.

85. Li, N., et al., *Nonlinear optical properties and memory effects of the azo polymers carrying different substituents.* Dyes and Pigments, 2011. **88**(1): p. 18-24.

86. Madruga, C., et al., *Birefringence dynamics of poly {1-[4-(3-carboxy-4-hydroxyphenylazo) benzenesulfonamido]-1, 2-ethanediyl, sodium salt} cast films.* Thin Solid Films, 2011. **519**(22): p. 8191-8196.

87. Ferreira, Q., et al., *Influence of ionic interactions on the photoinduced birefringence of Poly [1-[4-(3-Carboxy-4 Hydroxyphenylazo) benzene sulfonamido]-1, 2-ethanediyl, sodium salt] films.* Journal of nanoscience and nanotechnology, 2007. **7**(8): p. 2659-2666.

88. Yadavalli, N.S. and S. Santer, *In-situ atomic force microscopy study of the mechanism of surface relief grating formation in photosensitive polymer films.* Journal of Applied Physics, 2013. **113**(22): p. 224304.

89. Yadavalli, N.S., et al., *Soft matter beats hard matter: rupturing of thin metallic films induced by mass transport in photosensitive polymer films.* ACS applied materials & interfaces, 2013. **5**(16): p. 7743-7747.

90. Han, L.-H., T. Tang, and S. Chen, *Tuning the absorptions of Au nanospheres on a microshell by photo-deformation.* Nanotechnology, 2006. **17**(18): p. 4600.

91. Kim, H.-J., et al., *Dynamic sequential layer-by-layer deposition method for fast and region-selective multilayer thin film fabrication.* Langmuir, 2005. **21**(18): p. 8532-8538.

92. Lane, T.J., et al., *Dual-beam polarization interferometry resolves mechanistic aspects of polyelectrolyte adsorption.* Langmuir, 2008. **24**(19): p. 10633-10636.

93. Kett, P.J., et al., *Structural changes in a polyelectrolyte multilayer assembly investigated by reflection absorption infrared spectroscopy and sum frequency generation spectroscopy.* The Journal of Physical Chemistry B, 2009. **113**(6): p. 1559-1568.

94. Liu, Y., et al., *Film deposition mechanisms and properties of optically active chelating polymer and composites.* Colloids and Surfaces A: Physicochemical and Engineering Aspects, 2015. **487**: p. 17-25.

95. Liu, Y., K. Shi, and I. Zhitomirsky, *Azopolymer triggered electrophoretic deposition of MnO 2-carbon nanotube composites and polypyrrole coated carbon nanotubes for supercapacitors.* Journal of Materials Chemistry A, 2015. **3**(32): p. 16486-16494.

96. Luo, C., et al., *Preparation of C/Ni–NiO composite nanofibers for anode materials in lithium-ion batteries.* Applied Physics A, 2013. **113**(3): p. 683-692.

97. Gao, X. and R.C. Buchanan, *Solvent effects on properties of metallo-organic derived Ni/NiO thin films.* Thin Solid Films, 2011. **519**(18): p. 5899-5904.

98. Yuan, F., et al., *Synthesis, properties and applications of flowerlike Ni–NiO composite microstructures.* Journal of Materials Chemistry A, 2013. **1**(29): p. 8438-8444.

99. Luo, D. and I. Zhitomirsky, *Electrophoretic Deposition of Polyetheretherketone Composites, Containing Huntite and Alumina Platelets.* Journal of The Electrochemical Society, 2015. **162**(11): p. D3057-D3062.

100. Şen, F., S. Madakbaş, and M.V. Kahraman, *Preparation and characterization of polyaniline/Turkish Huntite-hydromagnesite composites.* Polymer Composites, 2014. **35**(3): p. 456-460.

101. Seki, Y., et al., *Effect of huntite mineral on mechanical, thermal and morphological properties of polyester matrix.* Composites Part B: Engineering, 2013. **45**(1): p. 1534-1540.

102. Cheong, M. and I. Zhitomirsky, *Electrodeposition of alginic acid and composite films.* Colloids and Surfaces A: Physicochemical and Engineering Aspects, 2008. **328**(1): p. 73-78.

103. Ferreira, Q., et al., *Long-term stability at high temperatures for birefringence in PAZO/PAH layer-by-layer films.* ACS applied materials & interfaces, 2012. **4**(3): p. 1470-1477.

104. Yi, Q. and G.B. Sukhorukov, *Externally triggered dual function of complex microcapsules.* ACS nano, 2013. **7**(10): p. 8693-8705.

105. Vasconcelos, D.C., E.H. Nunes, and W.L. Vasconcelos, *AES and FTIR characterization of sol–gel alumina films.* Journal of Non-Crystalline Solids, 2012. **358**(11): p. 1374-1379.

106. Corni, I., et al., *Electrophoretic deposition of PEEK-nano alumina composite coatings on stainless steel.* Surface and Coatings Technology, 2009. **203**(10): p. 1349-1359.

107. Erel-Unal, I. and S.A. Sukhishvili, *Hydrogen-bonded multilayers of a neutral polymer and a polyphenol.* Macromolecules, 2008. **41**(11): p. 3962-3970.

108. Shutava, T., et al., *pH responsive decomposable layer-by-layer nanofilms and capsules on the basis of tannic acid.* Macromolecules, 2005. **38**(7): p. 2850-2858.

109. Gulley-Stahl, H., et al., *Surface complexation of catechol to metal oxides: an ATR-FTIR, adsorption, and dissolution study.* Environmental science & technology, 2010. **44**(11): p. 4116-4121.

110. Jayaweera, P. and T. Jayarathne, *Acid/base induced linkage isomerization of alizarin red adsorbed onto nano-porous TiO 2 surfaces.* Surface science, 2006. **600**(22): p. L297-L300.

111. Kowalonek, J. and H. Kaczmarek, *Studies of pectin/polyvinylpyrrolidone blends exposed to ultraviolet radiation.* European Polymer Journal, 2010. **46**(2): p. 345-353.

112. Ibrahim, M., A. Nada, and D.E. Kamal, *Density functional theory and FTIR spectroscopic study of carboxyl group.* Indian Journal of Pure and Applied Physics, 2005. **44**(12): p. 911-917.

113. Hollingbery, L. and T.R. Hull, *The fire retardant behaviour of huntite and hydromagnesite–A review.* Polymer degradation and stability, 2010. **95**(12): p. 2213-2225.

114. Ye, L. and B. Qu, *Flammability characteristics and flame retardant mechanism of phosphate-intercalated hydrotalcite in halogen-free flame retardant EVA blends.* Polymer Degradation and Stability, 2008. **93**(5): p. 918-924.

115. Zeng, H.C., *Preparation and integration of nanostructured titanium dioxide.* Current Opinion in Chemical Engineering, 2011. **1**(1): p. 11-17.

116. RAVAGLIOLI, A., *Titanium Nitride Coating of Cobalt Chromium Coronary Stents: a SEM-EDS Analysis.* Interceram, 2010. **59**(2): p. 95-97.

117. Zürcher, S. and T. Graule, *Influence of dispersant structure on the rheological properties of highly-concentrated zirconia dispersions.* Journal of the European Ceramic Society, 2005. **25**(6): p. 863-873.

118. Džunuzović, E.S., et al., *Influence of surface modified TiO 2 nanoparticles by gallates on the properties of PMMA/TiO 2 nanocomposites.* European Polymer Journal, 2012. **48**(8): p. 1385-1393.

119. Radoman, T.S., et al., *Improvement of epoxy resin properties by incorporation of TiO 2 nanoparticles surface modified with gallic acid esters.* Materials & Design, 2014. **62**: p. 158-167.

120. Vigolo, B., et al., *An Experimental Approach to the Percolation of Sticky Nanotubes.* Science, 2005. **309**(5736): p. 920-923.

121. Vigolo, B., et al., *Macroscopic Fibers and Ribbons of Oriented Carbon Nanotubes.* Science, 2000. **290**(5495): p. 1331-1334.

122. Tummala, N.R. and A. Striolo, *SDS Surfactants on Carbon Nanotubes: Aggregate Morphology.* ACS Nano, 2009. **3**(3): p. 595-602.

123. Cheong, M. and I. Zhitomirsky, *Electrophoretic deposition of manganese oxide films.* Surface Engineering, 2009. **25**(5): p. 346-352.

124. Moon, J., et al., *Synthesis of nanocrystalline manganese oxide powders: Influence of hydrogen peroxide on particle characteristics.* Journal of Materials Research, 1999. **14**(12): p. 4594-4601.

125. Jacob, G.M. and I. Zhitomirsky, *Microstructure and properties of manganese dioxide films prepared by electrodeposition.* Applied Surface Science, 2008. **254**(20): p. 6671-6676.

126. Su, Y. and I. Zhitomirsky, *Electrophoretic deposition of graphene, carbon nanotubes and composite films using methyl violet dye as a dispersing agent.* Colloids and Surfaces A: Physicochemical and Engineering Aspects, 2013. **436**: p. 97-103.

127. MacLaren, D.C. and M.A. White, *Dye–developer interactions in the crystal violet lactone–lauryl gallate binary system: implications for thermochromism.* Journal of Materials Chemistry, 2003. **13**(7): p. 1695-1700.

128. Julien, C., et al., *Vibrational spectroscopy of lithium manganese spinel oxides.* Molecular Crystals and Liquid Crystals, 1998. **311**(1): p. 81-87.

129. Porkodi, K. and S.D. Arokiamary, *Synthesis and spectroscopic characterization of nanostructured anatase titania: a photocatalyst.* Materials Characterization, 2007. **58**(6): p. 495-503.

130. Gogotsi, Y. and P. Simon, *True Performance Metrics in Electrochemical Energy Storage.* Science, 2011. **334**(6058): p. 917-918.

131. Kötz, R. and M. Carlen, *Principles and applications of electrochemical capacitors.* Electrochimica Acta, 2000. **45**(15-16): p. 2483-2498.